OBSERVATIONS OF NIGHT AIRGLOW AT MT. ABU AND THEIR DISCUSSION

presented

by

B. S. DANDEKAR

for

the degree of

DOCTOR OF PHILOSOPHY

of

THE GUJARAT UNIVERSITY

June 1961

PHYSICAL RESEARCH LABORATORY

AHMEDABAD 9

(INDIA)

PREFACE

Aurorae are frequent in high latitudes, occasional in middle latitudes and rare in low latitudes. Night airglow is a feature common to all parts of the earth. Both aurorae and airglow have been the subjects of much study in high and middle latitudes. An observational station was set up at Mt. Abu (Geog.Lat.24°.6N, Long.72°.7E) by the Physical Research Laboratory, Ahmedabad, for the study of airglow in the tropics.

The present thesis incorporates the work done by the author on night airglow during the period January 1956 to December 1959.

Attention was concentrated on three wavelengths, (1) OI green line at 5577A, (2) OI red lines at 6300-6364A and (3) Na-D lines at 5890-5896A. In addition a narrow band region near 5300A, which does not contain any strong emission was studied to estimate the background radiation.

The method of photoelectric photometry with suitable optical filters was used for the intensity measurements of the airglow. The necessary equipment was built and maintained by the author. The photometers were calibrated against the light of a standard tungsten ribbon filament appropriately scattered by a screen. Regular observations were made in the direction of the pole and the data have been tabulated and analysed.

[The nocturnal variations of all these variations in different seasons are discussed and compared with those observed at a few other stations. The OI green line is found to exhibit a midnight maximum. The hour of occurrence of maximum is observed to shift a few hours with season. The intensity of the OI red lines is known to decrease rapidly in the first part of the night. This post twilight effect is prominent in autumn and less so in summer. The Na-D lines do not show any significant nocturnal variation.]

All-sky observations were taken on a few days. They give some information about the patchy nature of the airglow. The observations have also been used to make an estimate of the height of the emitting layer.

[Day to day changes in magnetic and solar activity are found to have little effect on the oxygen lines. However an enhancement of the intensity of the OI green line has been observed on a few nights following class 2 + and 3 solar flares.]

The variation in the intensity of the OI red lines has been found to depend on the critical frequency of the F layer. There seems also to be an effect of $h'F_2$ on the red airglow, the intensity of airglow decreasing with increase in h_pF_2 and h'F.

B.S. Dandekar

Countersigned. B.S.DANDEKAR

ACKNOWLEDGEMENTS.

I express my gratitude to Professor K.R.Ramanathan, Director of the Physical Research Laboratory for his kind guidance and encouragement in the work.

I thank my colleague Dr.R.V.Bhonsle for his help in the initial stages of building the airglow equipment. I am thankful to M/s. S.M.Bhat and V.G.Mazumbarkar for their kind assistance in the all-sky-survey observations of airglow at Mt.Abu and to M/s. S.K.Alurkar and Y.R.Waghmare for their help in photographic work.

Thanks are due to the Indian Council of Scientific and Industrial Research, and the Ministry of Education, Government of India for financial support.

References to other workers have been made at appropriate places.

B.S.Dandekar

(B.S.DANDEKAR)

CONTENTS

CHAPTER I

INTRODUCTION

CONTENTS

CHAPTER I

INTRODUCTION

1. Nature of the night-sky radiation

After sunset, the brightness of the sky decreases very rapidly. It becomes very weak when the sun is 18° below horizon. This is accepted as the conventional end of the twilight. During clear nights, the sky is not completely dark even in the absence of the moon, but emits a faint light in addition to the light from the stars. This emission is of atmospheric origin and is known as the airglow. The emission[1] produced by a clear night-sky on a horizontal plane is equal to that of a 25 candle power lamp at a distance of about 300 meters. The emission is known to occur throughout the twenty four hours. It is customary to refer to the night time emission as night airglow.

The airglow is extremely feeble and has a global character. In contrast, bright intermittent auroral displays are known to be frequent in high latitudes. The auroral lights are rarely observed at middle and low latitudes but airglow is always present. The auroral illumination is very intense, often perceptible even to the unaided eye, and exhibits structure unlike airglow.

The permanent global feature of the airglow permits its study at all latitudes and in different seasons. The fact that the airglow originates from a luminescence of the upper atmosphere is supported by the weak polarization observed by various investigators[2,3].

2. The airglow spectrum

(a) General description

The airglow spectrum covers a wide range from the ultraviolet to the infrared region. Its weak intensity necessitates the use of spectrographs of high light gathering power and highly sensitive plates. In addition lengthy exposures are needed to record weak emissions. The low dispersion and low resolving power introduce lack of precision in wavelength measurements. For accurate measurements of some lines an interferometer has been used. In the case of bands the intensity distribution and the appearance of a complete system of bands provide supplementary information. The identification of the airglow spectrum was hindered for a long time due to the fact that some of the more important emissions had not been produced in the laboratory.

In recent years starting from McLennan, the spectrum has been studied by Babcock, Cabannes and Dufay, Bappu[4], Meinel[5], Dufay and Dufay[6,7], Chamberlain[8,9], Chamberlain and Roesler[10], Gush and Jones[11], Krassovsky[12] and others.

The airglow spectrum consists of a number of lines and bands superposed on a continuous background.

(b) Lines

A green line at 5577A which also appears prominently in auroras is a permanent feature[13] of the airglow. It was detected by Campbell, measured by Slipher and its wavelength was confirmed by Babcock. Later McLennan and Shrum succeeded in producing it in the laboratory by passing an electrical discharge through a mixture of oxygen and an inert gas like argon.

In 1933 Slipher observed the oxygen red lines in the airglow in the form of a triplet near 6315A, which was later excited by Paschen in the laboratory. The accurate wavelength measurement was carried out by Cabannes and Dufay[14]. Of the triplet only two lines at 6300 and 6364A are of appreciable intensity. The lines 5577, 6300 and 6364 arise from forbidden transitions in excited oxygen atoms.

Along with the red lines Slipher noticed a yellow line at 5893A, which he attributed to sodium. Its presence was confirmed by Cabannes et al and by Bernard by interferometric measurements.

The N_2^+ band at 3914 A is known to be present in the twilight spectrum.

There is an emission at 6563 A which was attributed to H_α line by Vegard, and Elvey[15]. Its occasional presence in middle and high latitudes has been confirmed by Gartlein, ~~and~~ Prokudina, and Kvifte[16]. Its presence in low latitudes is however uncertain.

(c) Bands

The presence of Herzberg bands of O_2 in the ultra-violet was confirmed by the quantitative study by Dufay and Dejardin. Its presence was further supported by observations in the visible region by Barbier and Dufay, and by laboratory experiments by Broida and Gaydon[17,18].

The (0-1) band of atmospheric O_2 was discovered in the airglow spectrum by Meinel. The (0-0) band of O_2 is not observed at the ground as it is absorbed in the lower atmosphere during its passage.

The hydroxyl bands are known to be present in the airglow in the visible and more particularly in the near infrared region. Some of the infrared bands of OH are obscured due to the presence of telluric absorption bands of O_2 and H_2O. Beyond 2.5 μ region the thermal radiations of the lower atmosphere mask the OH bands.

(d) Continuum

In addition to atomic lines and molecular bands the airglow spectrum is known to contain a background of continuum. It starts below 4000 A and extends towards the red region. It is most prominent in the blue-violet region. Investigations by Rayleigh[19], Roach and Meinel[20] lead to the conclusion that some of the continuum is of extra-terrestrial origin. The view is supported by data collected from rocketborne photometers[21].

(c) <u>Comparison with auroral and twilight spectrum</u>

The auroral spectrum is known to be much brighter and richer in lines than the spectrum of the airglow. Most of the airglow features except the OH bands have been observed in the auroral spectrum. The essential difference in aurora and airglow lies in the degree of excitation of nitrogen bands. In the airglow spectrum, Vegard-Kaplan bands are the most intense, then come the 1st and 2nd positive systems. The negative bands of nitrogen have much more reduced intensity; and often they are absent. The order of intensity is reversed in the auroral spectrum.

The twilight spectrum is similar to that of the airglow. The N_2^+ band and the Na-D lines are enhanced in the twilight spectrum.

3. <u>Intensities of the airglow emission</u>

The transitions which give rise to the prominent features of the airglow have been summarised in table I. Their average relative intensities in the airglow spectrum are also given. A reference to table I shows that the OH bands are very intense in the airglow spectrum. This can be emphasised in the following way. "The quantal intensity of the OH bands would maintain a permanent midnight condition and there would be no night in the near infrared region".

Table I.*

Spectrum of the night airglow.

Source	Angstroms	Transition	Excitation potential eV	Relative intensity.	Mean absolute zenith intensity (Rayleighs).
OI	5577	$^1S_0 - {}^1D_2$	4.17	1	250
OI	6300	$^1D_2 - {}^3P_1$	1.96	0.6	150
OI	6363	$^1D_2 - {}^3P_0$			
Na I	5890	$^2P_{3/2} - {}^2S_{1/2}$	2.09	0.6	150
Na I	5896	$^2P_{1/2} - {}^2S_{1/2}$			
OH	In near infra-red from 4.4 μ to the visual.	v' = 9 to 1 v'' = 9 to 0	3.25	5000	10^6

* From the INSTRUCTION MANUAL No.IV, AURORA AND AIRGLOW, 1956.

At twilight the Na-D lines are approximately ten times stronger than in the airglow. The auroral intensities of the OI green line are very high and vary from one to several thousand kilo Rayleighs.

4. Height determination

The determination of the heights at which these emissions take place is very important for understanding of the mechanisms of these emissions.

In the case of aurora, prominent identifiable bright features can be made use of for determining the height. Simultaneous photographs from two or more stations against a star background was the method by Stormer and Vegard to determine the height of auroral emissions.

The feeble nature of the airglow and the lack of identifiable features hinder the use of a similar technique in measuring the heights of airglow radiations.

Most of the investigators have used a method known as Van Rhijn technique. It is based upon the empirical fact that the intensity of airglow increases in a systematic way from zenith towards horizon. It requires the comparison of intensities at two different zenith angles, and is valid only under some assumptions. In the beginning the method proved a failure, yielding heights ranging from 400 to 1000 km. Later Roach et al[22], Roach and Meinel[20], Barbier[23], the

Japanese group[24] and other workers[25] have partially succeeded in using this method with appropriate modifications.

The recent method of rocket borne airglow photometers[26,27,28] have yielded accurate and reliable information about the heights at which these radiations take place.

The results of these investigations have led to the following conclusions :

1. The OI green line is emitted at a height of about 100 km.

2. The OI red radiation emanates at a height more than 160 km, and is situated somewhere in the F region.

3. The OH bands and the Na-D lines are emitted from layers at 70 km to 90 km from the surface of the earth.

5. Temperature measurements from the airglow spectrum

The temperatures of the layers at which these radiations take place are determined from the spectral analysis by the use of two methods. One is by the measurement of the thickness of the spectral lines by an interferometer, and the other by a study of the intensity distribution of rotation-vibration molecular bands. The essential condition for the latter method is that departures from thermal equilibrium which may be caused by excitation mechanisms should have been dissipated before appreciable excitation takes place.

The Doppler width measurements[29,30,31] of OI green line yielded temperatures of 800 °K which is expected to exist at a height of 100 km.

The OI red lines yielded a temperature of about 700 °K.

The temperatures from the rotational structure[32] of the (0-1) atmospheric band of O_2 are as low as 150 to 200 °K.

Determinations of temperatures at levels of OH emissions have been made on the Meinel band[33] of vibration-rotation of OH. The T_{rot} for OH bands is estimated to be 230 °K.

For the Vegard-Kaplan bands of N_2 and the Herzberg bands[34,35] of O_2 the rotational temperatures are 230°K and 160-220 °K respectively.

The comparison of these results with those of the rocket panel data show that most of the airglow emissions (except the OI red lines) take place at or below the level of 100 km.

6. Excitation mechanisms

(a) Probable sources of excitation

Auroral excitation is supposed to originate in the energy of the incoming particles consisting of protons, electrons and neutral hydrogen atoms from the sun. The correlation between magnetic activity and aurora, similarity in their geographical distributions and the broadening of the H_α line have provided supporting evidence for such mechanism.

The excitation by incoming particles demands very high correlation of the airglow emissions with magnetic and solar activity, whereas the energy released in atmospheric motions is insufficient to produce the necessary excitations. The source for chemical energy or ionospheric processes is known to be solar radiation. The radiation is absorbed and stored during daytime and dissipated during night.

(b) Excitation mechanisms for individual emissions

The plausible excitation mechanisms which are responsible for the prominent features of the airglow are summarised in the following :-

(i) OI green line

Chapman[36] suggested that very large amount of energy is stored in the region of 100 km in the form of dissociation of oxygen atoms, a part of which is released in the form of radiation during night hours. The number of oxygen atoms present is $5 \cdot 10^{13}$ cm^{-3} and the recombination is of the order of 10^{12}. The reservoir is thus sufficient to maintain radiation throughout night. The extra energy available would be 5.11 eV in case of oxygen atoms which would suffice to produce the needed excitation. (The energy of excitation of $O(^1S)$ is 4.17 eV).

Chapman suggested the three body collision mechanism for the emission of the OI green line

$$O + O + O \longrightarrow O_2 + O(^1S)$$
$$\text{or} \quad O(^1D) \quad .. \quad .. \quad .. \quad .. \qquad (1)$$

The process would be very effective at a height of 100 km where the concentration of atomic oxygen is the highest.

The green line would be emitted according to

$$O(^1S) \longrightarrow O(^1D) + h\nu \ (5577 \text{ Å}) \quad .. \quad .. \quad .. \qquad (2)$$

The process is able to explain the observed intensity of the OI green line but is unable to explain its diurnal and seasonal variation.

(ii) <u>OI red lines</u>

The reaction (1) would also give rise to the OI red radiation. Relation (2) will increase the population of

$O(^1D)$. In such case OI red lines would be stronger than the green line or the deactivation process would be effective.

According to Bates and Dalgarno[37], and Seaton[38], the suppression of OI red lines at this altitude would be due to

$$O(^1D) + O_2 \rightleftarrows O(^3P_2) + O_2^* \quad .. \quad .. \quad .. \qquad (3)$$

which is almost an exact energy resonance. However the inverse process should be taken into account.

The dissociative recombination[39] would be important according to

$$O_2^+ + e \longrightarrow O + O(^1D) \quad .. \quad .. \quad .. \quad .. \quad .. \qquad (4)$$

which would partially account for the OI red radiation.

The O_2^+ ions would be formed either by charge transfer[39,40]

$$O^+ + O_2 \longrightarrow O_2^+ + O(^3P) \quad .. \quad .. \quad .. \quad .. \quad .. \qquad (5)$$

or by ion-atom interchange

$$O^+ + O_2 \longrightarrow O_2^+ + O(^3P) \quad .. \quad .. \quad .. \quad .. \quad .. \qquad (6)$$

The emission of OI red lines takes place according to

$$O(^1D) \longrightarrow O(^3P) + h\nu \ (6300 \text{ and } 6364 \text{ Å}) \quad .. \qquad (7)$$

The other possibility of excitation is by direct electron impact

$$e + O(^3P) \longrightarrow e + O(^1D) \quad .. \quad .. \quad .. \quad .. \quad .. \quad (8)$$

(iii) Na-D lines

The two body chemical processes of substitution type

$$XY + Z \longrightarrow X' + YZ' \quad .. \quad .. \quad .. \quad .. \quad .. \quad .. \quad (9)$$

would be very important in the case of rare constituents like sodium.

Chapman suggested the reaction

$$NaO + O \longrightarrow O_2 + Na(^2P) \quad .. \quad .. \quad .. \quad .. \quad .. \quad (10)$$

but the reaction is known to be endothermic.

Bates and Nicolet[41] suggested an alternative possibility

$$NaH + O \longrightarrow OH + Na(^2P) \quad .. \quad .. \quad .. \quad .. \quad (11)$$

or by Bates

$$NaH + H \longrightarrow H_2 + Na(^2P) \quad .. \quad .. \quad .. \quad .. \quad .. \quad (12)$$

Both the reactions are known to be exothermic.

The emission of Na-D lines would be according to

$$Na(^2P) \longrightarrow Na(^2S) + h\nu \quad (5890 \text{ and } 5896 \text{ Å}) \quad .. \quad .. \quad .. \quad (13)$$

(iv) OH bands

For the Meinel hydroxyl system Bates and Nicolet[42], and Herzberg suggested the following sequence :

$$OH + O \longrightarrow H + O_2 \quad .. \quad .. \quad .. \quad .. \quad .. \quad .. \qquad (14)$$

$$H + O_3 \longrightarrow O_2 + OH^*(v' \leq 9) \quad .. \quad .. \quad .. \quad .. \qquad (15)$$

The existence of such process has been proved by the laboratory experiments carried out by McKinley and his associates[43]. They succeeded in producing in the laboratory an OH spectrum in which the distribution of intensity of the bands in the infrared region was similar to that of the airglow.

7. Need for study of airglow in tropics

From the forgoing discussion one can conclude that the study of airglow and aurorae is a valuable means of obtaining a better understanding of the upper atmosphere. A considerable amount of work has been done, at high and middle latitudes. Aurorae are quite rare at low latitudes but night airglow is always present. But its study at low latitudes has received little attention. An observation station was therefore started at Mt. Abu (India) by the Physical Research Laboratory, Ahmedabad, in December 1955 for the study of airglow in the tropics.

8. Climatic conditions of Abu

The geographic coordinates of Abu are Lat. 24°.6N, Long.73°.72, (Geomag.lat.15°N). It has an elevation of 4000 ft above mean sea level. The presence of a local generating station permits the use of electrical equipment for the airglow observations. The site of observations is little affected by city lights.

The sky conditions are quite favourable for the observations from October to May. In the monsoon season, the sky usually remains overcast, with frequent occurrence of rain-showers. These conditions do not allow any chance of observation from June to September.

9. Programme of airglow study

Attention was concentrated on three radiations, OI green line at 5577 A, OI red lines at 6300-6364 A and the Na-D lines at 5890-5896 A. The method of photoelectric photometry with optical filters was used. Two photometers were built, one consisting of an RCA 931-A photomultiplier with 5577 and 5300 A interference filters, the other comprising of an EMI 6095 photomultiplier and 6300, 5890 A filters. The former allowed the study of the OI green line and the estimation of the background emission in 5300 A region. The latter permitted the study of OI red and Na-D lines.

The observations on these radiations were usually recorded towards the celestial pole on most of the nights when there was no moon.

The other part of the programme consisted of scanning the whole sky at regular intervals with an EMI 6095 photometer, for the study of spatial and temporal variations of the radiations. From November 1958 to April 1959 observations were obtained on 15 nights.

In addition an automatic scanning unit operating in the meridian plane was constructed for the study of the variations of OI green line over the S.A belt.

10. The scope of the thesis

The thesis incorporates the study of airglow made by the author at Mt.Abu under the auspices of the Physical Research Laboratory, Ahmedabad.

The equipment for the airglow observations was constructed and maintained by the author. The results presented here relate to observations from December 1955 to December 1959. These have proved useful for the following problems :-

(1) Diurnal and seasonal variations of airglow.

(2) The variations of airglow (5577 A) in different directions of the sky.

(3) The determination of the height of the emitting layer (5577 A radiation), and

(4) Correlations between airglow activity and other geophysical phenomena.

The thesis discusses the results which emerged from the study. The first chapter reviews the present position of the subject. The second chapter describes the construction and calibration of the equipment used for recording the radiations. In the third chapter the diurnal and seasonal variations are discussed and compared with those at a few other stations. The remaining chapters deal with the variations of airglow all over the sky, the height of the emission layer and the correlations between airglow activity and other phenomena.

REFERENCES

	Ratcliffe J.A.	1960	Physics of the upper atmosphere, Academic Press, London.
1.	Dejardin G.	1936	Rev.Mod.Phys., 8, 1.
2.	Dufay J.	1929	J.de Phys.et rad., 10, 219.
3.	Bricard J. and Kastler A.	1950	Ann de Geophys., 6, 286.
4.	Bappu M.K.V.	1950	Astrophys.J., 111, 201.
5.	Meinel A.B.	1950	Astrophys.J., 111, 555.
6.	Dufay M. and Dufay J.	1955	Ann de Geophys., 11, 209.
7.	Dufay M. and Dufay J.	1951	C.R.Acad.Sci., 232, 1293.

8.	Chamberlain J.W.	1955	Astrophys.J., __121__, 277.
9.	Chamberlain J.W.	1955	Astrophys.J., __121__, 713.
10.	Chamberlain J.W. and Roesler F.L.	1955	Astrophys.J., __121__, 541.
11.	Gush H.P. and Jones A.V.	1955	J.Atmos.Terr.Phys., __7__, 285.
12.	Krassovsky V.	1956	The airglow and the aurorae, Pergamon Press, p.36.
13.	Rayleigh L.	1928	Proc.Roy.Soc., __119__, 11.
14.	Cabannes J. and Dufay J.	1956	The airglow and the aurorae, Pergamon Press, p.73.
15.	Elvey C.T.	1950	Astrophys.J., __111__, 432.
16.	Kvifte G.	1959	J.Atmos.Terr.Phys., __16__, 252.
17.	Broida H.P. and Gaydon A.G.	1954	Proc.Roy.Soc., __A 222__, 181.
18.	Gaydon A.G.	1956	The airglow and the aurorae, Pergamon Press, p.262.
19.	Rayleigh L.	1920	Nature, __106__, 8.
20.	Roach F.E. and Meinel A.B.	1955	Astrophys.J., __122__, 530.
21.	Heppner J.P. and Meredith L.H.	1958	J.Geophys.Res., 63, 51.
22.	Roach F.E., Megill L.R., Rees M.H. and Marovich E.	1958	J.Atmos.Terr.Phys., __12__, 171.
23.	Barbier D.	1957	Ann de Geophys., __13__, 217.
24.	Huruhata M. and Tohmatsu T.	1957	Rep.Ionos.Res., Japan, __11__, 11.
25.	Elsasser H. and Siedentopf H.	1956	The airglow and the aurorae, Pergamon Press, p.27.
26.	Berg O.E., Koomen M.J., Meredith L. and Scolnik R.	1956	J.Geophys.Res., __61__, 302.

27.	Berg O.E., Koomen M.J., Meredith L. and Scolnik R.	1956	J.Geophys.Res., 61, 302.
28.	Tousey R.	1958	Ann de Geophys., 14, 186.
29.	Work D.Q. and Stone J.M.	1955	Nature, 175, 254.
30.	Armstrong E.B.	1953	J.Atmos.Terr.Phys., 3, 274.
31.	Phillips J.G.	1956	The airglow and the aurorae, Pergamon Press, p.67.
32.	Meinel A.B.	1950	Astrophys.J., 112, 464.
33.	Meinel A.B.	1950	Astrophys.J., 112, 120.
34.	Swings P.	1943	Astrophys.J., 97, 72.
35.	Chamberlain J.W.	1955	Astrophys.J., 121, 277.
36.	Chapman S.	1931	Proc.Roy.Soc., A132, 353.
37.	Bates D.R. and Dalgarno A.	1954	J.Atmos.Terr.Phys., 5, 329.
38.	Seaton M.J.	1955	Ann de Geophys., 11, 232.
39.	Bates D.R. and Massey H.S.W.	1947	Proc.Roy.Soc., 192, 1.
40.	Nicolet M.	1954	Phys.Rev., 93, 633.
41.	Bates D.R. and Nicolet M.	1950	J.Geophys.Res., 55, 235.
42.	Bates D.R. and Nicolet M.	1950	J.Geophys.Res., 55, 301.
43.	McKinnely J.D., Garvin D. and Boudart M.J.	1956	The airglow and the aurorae, Pergamon Press, p.264.

CHAPTER II

PHOTOMETRY OF AIRGLOW

CONSTRUCTION AND CALIBRATION OF PHOTOMETER

CONTENTS

9. Calibration of the photometers.

(a) General considerations.

(b) Methods of calibration.

(c) Experimental set up.

(d) The derivation of the formula.

10. Contamination due to background and its elimination.

REFERENCES.

CHAPTER II

PHOTOMETRY OF AIRGLOW

CONSTRUCTION AND CALIBRATION OF PHOTOMETER

1. General description

It is known that even in low and middle latitudes where auroras are rare, there is a permanent faint airglow coming from excited atoms and molecules in the upper atmosphere and that this glow undergoes periodic and nonperiodic variations. For the detection and identification of the spectrum of the airglow, spectrographs with large apertures have to be employed and long exposures have to be given. The study of the short period changes in the intensity of the airglow has in recent years been greatly facilitated by the use of the photomultipliers and appropriate interference filters.

In the work done by the author at Mount Abu attention was concentrated on the measurement of the intensities of light on three wavelengths (1) the oxygen green line OI 5577 A, (2) the oxygen red lines OI 6300-6364 A and (3) the sodium yellow lines (Na-D 5890-5896 A). In addition, the radiation in a narrow band at 5300 A where there are no important lines was also studied for estimating the continuous background radiation from stars.

Figure 1 shows a block diagram of the equipment used. The photometer converts the light signal from the sky to an electrical current. The high-tension voltage for the phototube is obtained from a stabilised H.T. supply. The output voltage of the phototube is amplified by a three-stage d.c. amplifier. The filaments of the amplifier valves are heated from a 6 V accumulator to ensure good stability. The power for the amplifier valves is derived from a low tension electronically stabilised power supply. The amplified signal is finally fed to a 0-1 mA d.c. Evershed pen recorder.

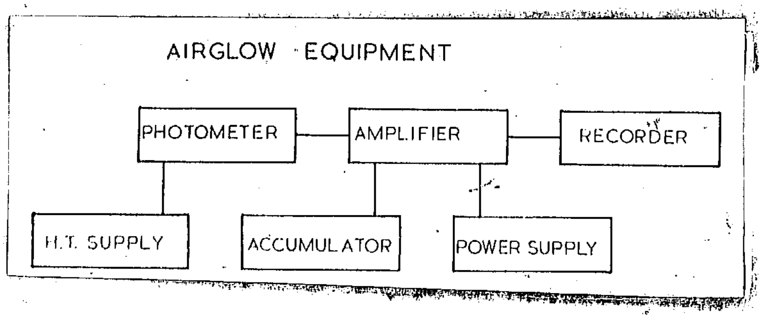

Fig.1. Schematic diagram of the airglow equipment.

2. Airglow photometer

The different constituents of the airglow equipment are described in detail in the following.

(c) Basic operation of a photomultiplier

The basic operation of a photomultiplier tube is shown in Figure 2. It consists of a photocathode, a series of target electrodes or dynodes at increasing potentials and a collector.

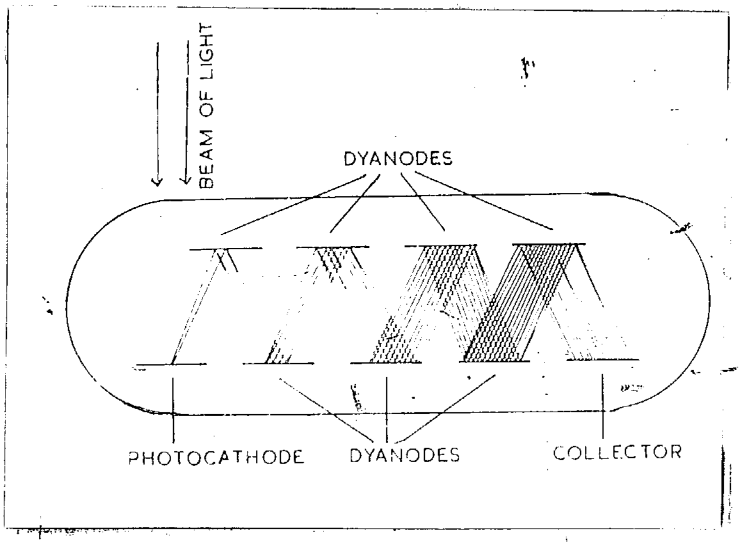

Fig.2. Operation of a photomultiplier.

When the light beam falls on the photocathode, a photocurrent i_0 is drawn from it to the first target. The target emits a secondary electron current i_0R where R is the secondary emission ratio of the surface. This current in turn strikes the second target and ejects from it a current i_0R^2. Thus for n target-electrodes the current reaching the collector is i_0R^n. So a photomultiplier with 10 dynodes and each with an yield of R = 4 has an output current one million times as great as the current leaving the photocathode.

Usually all electrons leaving one target do not reach the successive target. This reduces the gain of the photomultiplier. This is avoided by an appropriate design of the photomultiplier. There are two classes of photomultipliers : (1) magnetic multiplier phototubes and (2) electrostatic multiplier phototubes.

In magnetic multiplier phototubes the photocathode and the dynodes are all in one plane. The increasing voltages are applied to the successive dynodes and a magnetic field is maintained by a pair of soft iron pole pieces outside the tube envelope. Even though the performance of the magnetic multiplier is satisfactory, the requirement of the external magnetic field makes the multiplier unit complicated and unwieldy.

The electrostatic multiplier consists of a sequence of secondary emission activated fine mesh screens at increasing potentials, a transparent cathode at one end and a collector at the other. For more efficiency and compactness, instead of the screens, electrodes with appropriate shapes are used for guiding of electrons from cathode to cathode. A more compact multiplier phototube is obtained by arranging the electrodes in a circular array as in an RCA 931-A phototube.

(b) Dark current of the multiplier

A multiplier will pass a certain amount of current when the voltage is applied to the dynodes even when the photocathode is unilluminated. Such dark currents have to be allowed for when the device is used for the measurement or detection of very weak lights.

The sources of the dark current are (1) leakage between the electrodes both inside and outside the envelope, (2) thermionic emission from the photocathode to dynodes which is multiplied along with the signal light current, (3) the current generated by the positive ion impact on the photocathode and dynodes, which is augmented by field emission currents from the projecting points of electrodes. The ohmic leakage is reduced by the proper design of the multiplier. The dark current due to thermionic emission can be reduced by operating the multiplier at a lower temperature, for instance by immersing it in solid CO_2 or in liquid air. To avoid instability due to the dark current arising from the impact of a positive ion on photocathode or dynodes, the dynodes are fed with appropriate voltage.

(c) Photometers used for airglow observations

For the night airglow observations two photomultipliers were used (1) RCA 931-A and (2) EMI 6095. RCA 931-A has a side on photocathode with nine stages of multiplication. The multiplier has a maximum response at 4000 A. Its typical sensitivity is 20 A/L with 100 v per stage. EMI 6095 is an end on photomultiplier with a large size photocathode and eleven stages of multiplication. The sensitivity at 100 v per stage is 300 A/L.

RCA 931-A was used for studying the regions 5300 and 5577 A. EMI 6095 which has a higher gain and higher relative response was used for the study of 5300, 5577, 5893, and 6300 A regions.

For the RCA 931-A photomultiplier the voltage per stage was -95 v with -100 v between the final dynode and the anode. The EMI 6095 photomultiplier was operated at -1150 v, with the voltage between the final dynode and anode, double the voltage per stage.

Figure 3(a) shows a schematic diagram of the photometer in which an RCA 931-A photomultiplier is the sensing element. The phototube is housed in an earthed copper tube T. B is a box which contains a chain of resistances appropriately connected to an H.T. supply to furnish appropriate voltages to the dynodes of the phototube P. S is a shutter which can cut out the light from the phototube and can be operated by the knob K. The tube T with the box B is fitted in a wooden box W. Two filters F_1 and F_2, one transmitting a narrow band near 5577 A and the other a band near 5300 A are mounted on the disc D. The disc D is fitted on the axle X and can be rotated by a motor through intermittent gears G. When exposed, the light falls on the phototube through one of the filters for about 2½ minutes, one after the other. The disc acts as a shutter. When the shutter cuts off the light, the dark current level is recorded. The projecting cylindrical tube contains the aperture A, which defines the angle subtended by the photometer. The inside of the tube is coated with lampblack. The photometer covers a circular field of 11°.2 diameter. The plugs for the H.T. voltage and the output signal are mounted on the side of the box B.

Fig.3(a) Polar airglow photometer used at Mt.Abu for 5577 and 6300 A radiation.

The wooden box is mounted on a platform which can be suitably turned so as to point the photometer towards the celestial pole.

Fig.3(b). Alt-azimuth airglow photometer for the airglow observations at 5300, 5577, 5893 and 6300 A.

Figure 3(b) show the other photometer which uses an EMI 6095 photomultiplier. The lens L with the focal length 4" and aperture 3" forms the objective. It is fitted in such a way that the photocathode lies in its focal plane. S is a shutter which can cut off the light from the phototube P. A small radioactive source is fitted in the shutter S. Two interference filters are used, one for selecting the sodium yellow lines at 5890-5896 A and the other for the OI red lines 6300-6364 A. The filters are rotated by a motor M through the gears G. The photometer is provided with an alt-azimuth mounting. S shows the altitudinal scale and ϕ shows the azimuthal scale. The aperture A situated just above the photocathode defines the cone of reception of the photometer. It covers a circular field of 7°.2 diameter.

For routine observations, the photometer was turned towards the celestial pole.

For the full-sky scanning observations the disc D could be replaced by another disc which could hold four filters. The motor M was removed and the filters could be changed manually by rotating the axle X. A metal knob with notches was mounted on the axle X and was held rigid by a spring mounted on the cover C. This system was used to maintain the appropriate position of the filter above the aperture A.

(d) <u>Characteristics of optical filters</u>

Figure 4 represents the transmission characteristics of the optical interference filters. Filters I and II are used with the RCA 931-A phototube and III to VI with the EMI 6095 photomultiplier. The continuous curve represents the dependence of the transmission of the filter upon wavelength, whereas the dotted curve shows the transmission of the filter multiplied by the response of the photomultiplier. An OY 18 Corning glass filter is used in conjunction with the 5577 A filter (II) to cut off some of the unwanted yellow region of the spectrum. Along with 5890 A filter (V) OY_1 is used to cut off the red region and with 6300 A filter (VI) a 'plastic red' filter is used to cut off the unwanted yellow region. The use of these appropriate filters allows the selection of the oxygen green line, sodium yellow lines and the oxygen red lines respectively. The 5300 A filter allows the estimation of the background radiation.

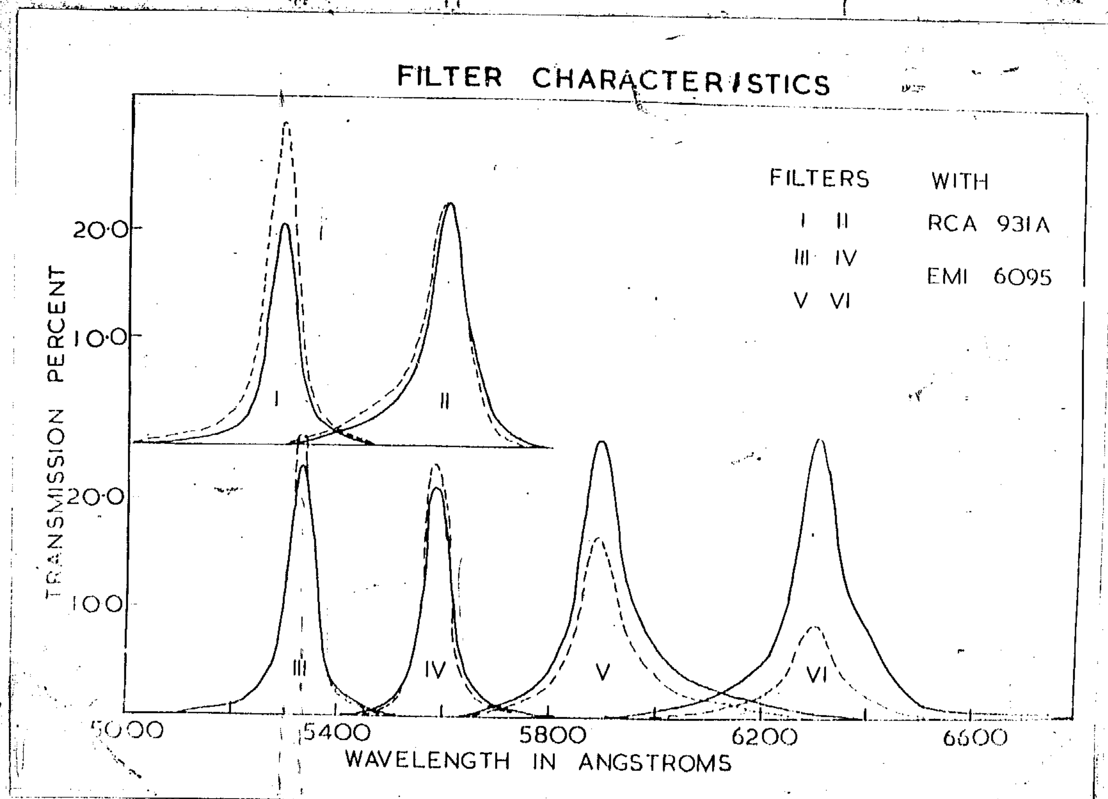

Fig.4. Dependence of filter transmission on wavelength.

The interference filters used were made by Messrs Barr and Stroud. Their peak transmissions and the band widths are summarised in table I.

Table I

Filter characteristics

Filters	I	II	III	IV	V	VI
1. Filter combination.	5300A inf.	5577A inf. +OG16	5300A inf.	5577A inf.	5893A inf. +OY1	6300A inf. +plastic red
2. Emission selected		OI 5577A		OI 5577A	Na-D 5890-5896A	OI 6300-6364A
3. Peak transmission	0.203	0.223	0.231	0.219	0.253	0.237
4. Transmission at selected wavelength	0.190	0.190	0.192	0.210	0.255	0.237
5. Half transmission band-width in A	55	30	60	60	35	30
6. Equivalent band-width* in A	21	135	152	30	150	140
7. Photomultiplier used	RCA 931-A	EMI 6095				

* Equivalent band-width is defined by $W = \frac{\int_{\lambda_1}^{\lambda_2} t_\lambda R_\lambda \, d\lambda}{T_{em} R_{em}}$

t_λ - transmission of the filter at wavelength λ.

R_λ - relative response of the photomultiplier at λ.

T_{em} - transmission of the filter at the emission wavelength.

R_{em} - response of the photomultiplier at the emission wavelength.

3. The [illegible] amplifier

(a) General considerations

The output current of the photomultiplier has usually a very small magnitude. For amplifying weak signal currents of this order, the amplifier should take a sufficiently high resistance in the grid circuit, so as to build a sufficient voltage signal across it. This demands the introduction of high resistances of the order of 1000 megohms in the grid circuit of an ordinary d.c. amplifier. But in the normal amplifier the grid current itself is of the same order as that of the current involved in the present measurements. This offsets the usability of normal amplifiers. So it is essential to reduce the grid current to a minimum.

The grid current may be due to any one of the following phenomena :-

1. The cathode of the valve can emit positive ions, which flow to the grid.
2. The electrons flowing from grid to plate can ionize the residual gas left in the tube, in which case some of the positive ions produced will flow to the grid.
3. The plate or some part of the tube may emit electrons, which is known as photoelectric effect.
4. The electrons impinging on the plate may have enough energy to cause the emission of soft X-rays. These

in turn can bombard the grid and emit electrons.

5. Electrons may reach the grid from cathode by virtue of the finite velocity with which they are emitted.

6. Leakage currents can occur over the inside or the outside of the tube.

All these sources of grid current should be minimised so that the amplifier can take a high resistance in its input circuit. The use of a special tube maintained under specific conditions for reducing all the above mentioned sources of grid current is known as electrometer operation.

(b) Design of the amplifier

Figure 5 shows the circuit of the three stage d.c. amplifier. The first stage of this consists of the electrometer operation followed by two successive push-pull stages. For the electrometer operation an acorn tube 954 is used. The operating conditions are as mentioned below.

The plate is run at low voltage of +6 v. The screen grid is operated at + 15 v. The filament of the valve is rated at 4.2 v. The conventional control grid is connected to the filament, the suppressor grid is biased at - 3 v, and used as the control grid. For reducing the surface leakage current the high meg resistor and the tube with its base are cleaned with petrol. These are kept dry and free of moisture by means of a desiccator. The effects of stray electric and magnetic fields are eliminated by properly shielding the amplifier. All the connection leads are run as direct as possible and are made by use of shielded wire. In the input circuit a glass sealed high megohm Victoreen resistor is employed.

To suppress the steady part of the plate current of the 954 tube from further amplification, the electrometer tube is put in a Wheatstone's bridge as shown in the figure.

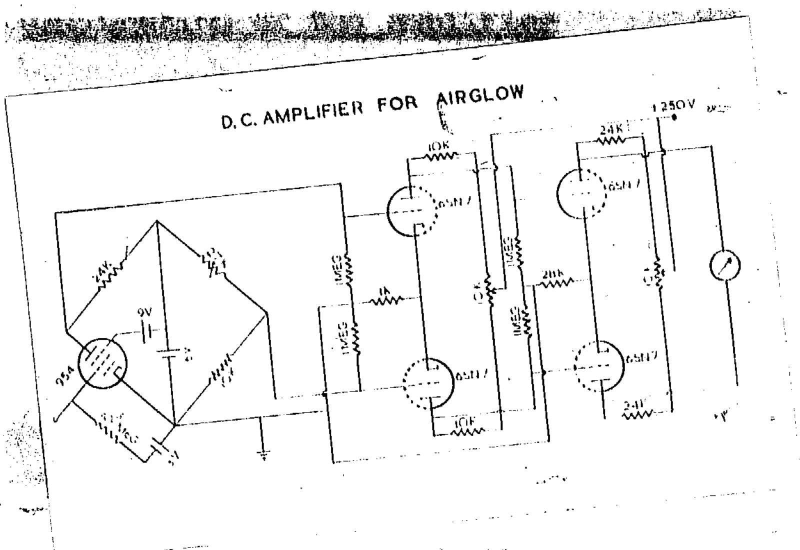

Fig.5. Three stage d.c. amplifier.

The tube with its plate load forms one arm of the bridge and a potential divider with a variable resistance forms the other arm. The double ended output of the bridge circuit is amplified by using two 6SN7 push-pull stages. The use of the push-pull amplifier minimises the harmful changes introduced due to the change in the filament and the plate voltages of the valves. The filaments of the valves are heated from a 6 V accumulator to ensure better stability. The potential divider in the plate circuit of the push-pull stages enables an appropriate matching of the two sections of each amplifier stage. The common resistance in the cathodes of each stage furnishes the necessary bias. It also provides a negative feed back and improves the stability of the amplifier.

(c) <u>Calibration of the amplifier</u>

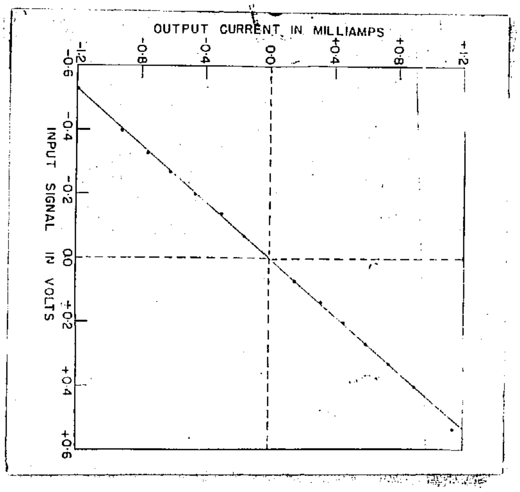

Fig.6. Calibration curve of the d.c. amplifier.

The amplifier was tested to find its sensitivity and range of linearity by feeding an arbitrary signal from a 2 V accumulator. The results are presented in Fig.6. It is seen from the graph that the amplifier is linear in the range ± 1 mA. The overall current gain of the amplifier is

$2.3 \cdot 10^{-3} / 10^{-9} = 2.3 \cdot 10^{6}$.

4. The recorder

The output signal from the d.c. amplifier is fed to a pen recorder. It is a recording millimeter with 0-1 mA full scale sensitivity, obtained from Evershed and Vignoles Co., England. It has a synchronous motor drive, with the chart speed of 1 inch per hour. It has a time constant of the order of one second, but is slightly variable with the magnetic damping arrangement provided in the instrument.

5. The H.T. supply

The high tension needed for the dynodes of the photomultiplier is derived from an H.T. supply. Its circuit diagram is shown in Fig.7. The power-pack portion of the supply consists of two 5 R 4 valves forming a voltage doubler circuit. The input a.c. voltage is 600 v. The voltage doubler furnishes about 1300 v d.c. The remaining part of the circuit makes up the regulating system. The 6L6 tube plays the role of a variable resistance. The high gain, sharp cut off pentode 6SH7 forms the amplifier part and works on the principle of degenerative circuit. The plate resistance of the amplifier is connected to the cathode of 6L6 tube, and only a part of its voltage is fed to the grid of 6L6. The reference voltage for the amplifier is obtained from a VR 150 tube. The current for the VR tube is provided from the input side of the regulating circuit. A part of the output voltage is tapped from the bank of resistances and is fed to the grid of the amplifier. This serves as an error voltage. The screen of the amplifier is maintained at a steady potential from the output side as shown in the figure.

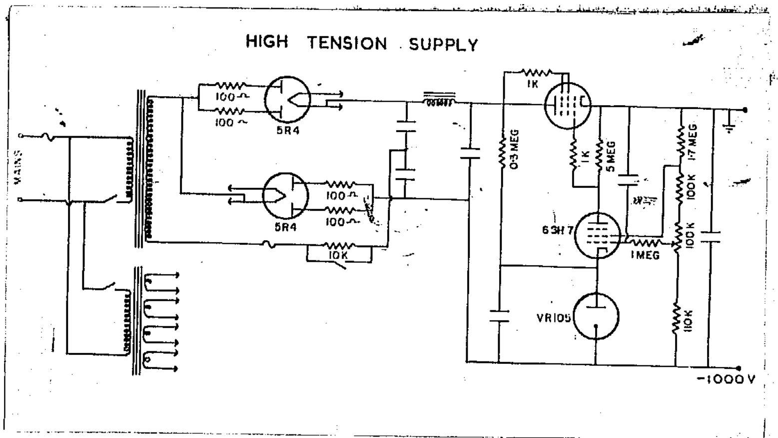

Fig.7. Electronically stabilised H.T. supply for the photomultiplier.

The working of the amplifier

The rise in the output side increases the grid voltage of the amplifier. This reduces the current in the anode circuit, thus the anode potential falls. The fall in the anode potential reduces the grid voltage of the variable resistance tube, thereby reducing the current through the load. The fall in the current increases the drop across the variable resistance tube, which causes a drop in the output voltage, thus offsetting the initial increase. Thus the amplifier provides a negative feedback between the input and the output circuits of the variable resistance tube, which tends to keep its output constant.

The H.T. supply has a ripple voltage of 10 mV at an output voltage of 1000 v. The variable resistance in the bleeder chain provides a range of 50 v on either side.

6. Power supply for the amplifier
of th ... at the

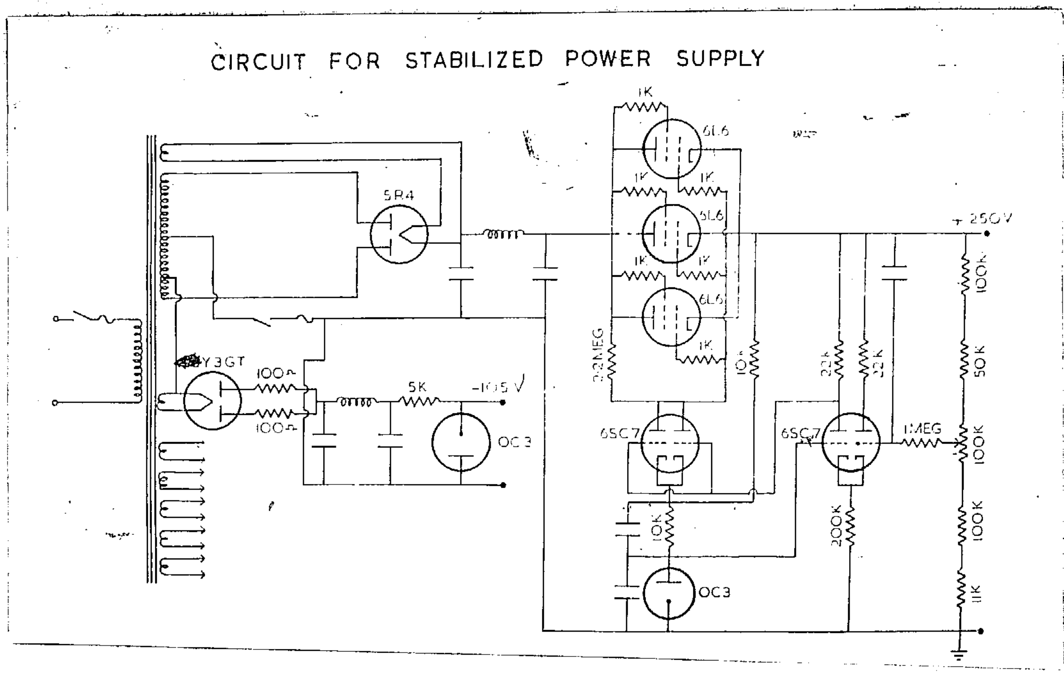

Fig.8. Power supply for airglow amplifier.

An electronically stabilised model 50 power supply circuit[1] was suitably modified to deliver 250 v d.c. for furnishing the power to the plates of the amplifier. Fig.8

shows the circuit of this power supply. The full wave rectification by a 5Y4 valve of 350-0-350 v a.c. with choke and condensers form the power pack of the supply. The remaining constitutes the stabilisation circuit. Three 6L6 valves are used in parallel as the variable resistance to get sufficient current from the output side. This variable resistance is controlled by a two stage amplifier. The first stage consists of a difference amplifier followed by another stage of amplification. The reference voltage to the grid of the difference amplifier of 6SJ7 valve is obtained from a VR tube. The current for VR tube OC3 is furnished from the plate side. This ensures that the reference voltage will not be subjected to the changes caused by the varying current through the VR tube. The error voltage for the second grid of the difference amplifier is tapped from the output side. A steady voltage is fed to the plates of the difference amplifier from the cathode side of the variable resistance. The signal of the difference amplifier is further amplified by another 6SJ7 valve. The plate load of this amplifier is returned to the power-pack side. This allows the potential of the grid of 6L6 to approach that of its cathode without any reduction in the current of the amplifier stage, thus the gain of the amplifier does not reduce. The use of the difference amplifier reduces the drifts of the supply voltages which are due to the changes in the heater voltages. The power supply has a low r.m.s. ripple of 3 mV for an output voltage of 250 v.

7. Stability of the airglow equipment

The stability of the airglow equipment was checked by the use of proper radioactive sources. For RCA 931-A photometer the procedure was to expose the photometer to the radioactive source and note the deflections caused for both the filters, at the beginning and at the end of the observations. For EMI 6095 photometer, the photometer could be directly exposed to the radioactive source by means of the shutter S (in Fig.3b). The observed intensities were then appropriately corrected according to the deflections caused by the signal from the radioactive source.

8. Sample records

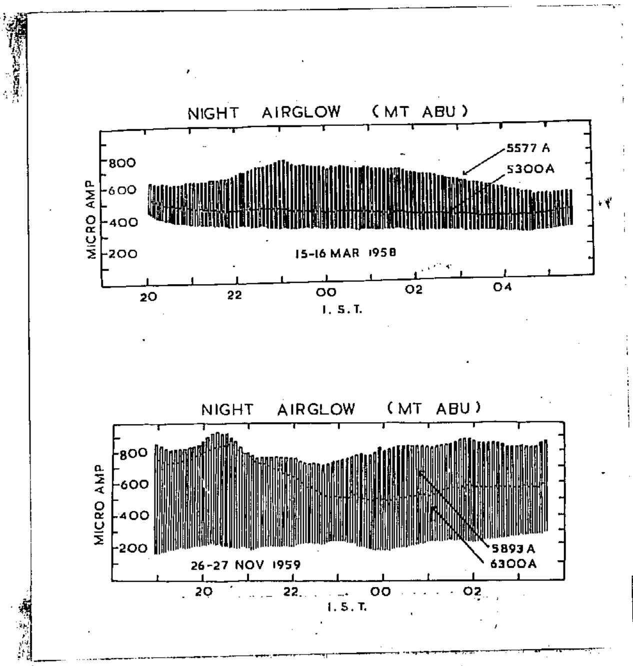

Figs.9(a) & (b). Sample records of nocturnal variations of the airglow at 5300, 5577, 5893 and 6300 A.

Figs.9(a) and 9(b) show the sample records of the observations taken at Mount Abu with these photometers.

In Fig.9(a) the curve with higher amplitude refers to the intensity of the OI green line and the one with lower amplitude to 5300 A region. The record in Fig.9(b) with higher amplitude relates to the Na-D lines and the other with the lower amplitude to the OI red lines. The smaller amplitude of the OI red lines is due to the lower response of the photomultiplier at that wavelength.

9. Calibration of the photometers

(a) General considerations

For the intercomparison of the observations at different stations, it is advisable to express all the observations in some standard unit. Therefore Hunten, Roach and Chamberlain[2] suggested that the intensities should be expressed in a unit 'Rayleigh'. The Rayleigh is defined by an expression $R = 4\pi B$ where B refers to the surface brightness of the sky in 10^6 quanta / cm^2 . sec. sterad.

(b) Methods of calibration

There are three methods to calibrate the airglow photometers. These are :

1. Calibration from star deflections.

2. Calibration from the mean zenith intensity of the integrated starlight and the zodiacal light, and

3. Calibration against a standard source, whose spectral energy distribution is known.

The first two methods have been discussed in detail by Roach[9]. It should be noted that both these methods involve some basic assumptions, and demand quite a large number of observations. The last mentioned method is reproducible and involves fewer assumptions. This method was used for calibrating the airglow equipment.

(c) Experimental set up

The photometers were calibrated against a tungsten W-4 type ribbon filament lamp obtained from Messrs Philips. The arrangement of the calibration set up is shown schematically in figure 10. S is a screen coated with magnesium oxide. F is the tungsten filament lamp which illuminates the screen. The filament is heated by a d.c. current which is measured with accuracy. The colour temperature of the filament is found out from its calibration curve from the knowledge of the heating current. The slit T just above the lamp defines the area of the filament which illuminates the screen. P is the photometer kept at a distance D from the screen and it covers a small portion of the screen.

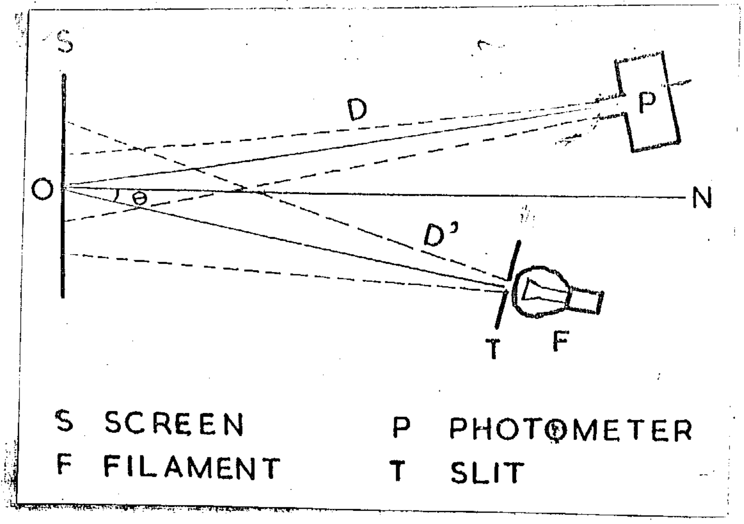

Fig.10. Experimental set up for the calibration of the airglow photometer against a standard tungsten filament lamp.

For taking the observations the airglow equipment was run at the usual voltages, with the only difference that the photometer was exposed to the MgO screen instead of the sky. For a known temperature of the filament the signal deflections were noted for different distances D' of the filament from the screen. Appropriate neutral filters were introduced on the photometer aperture to obtain reduced illumination from the screen. The observations were taken with an Avo 8 meter for the sake of convenience and accuracy. Two different temperatures of the lamp were used for calibration purposes. All the observations are summarised in tables IIa and IIb.

The last two columns of these tables give the product $D'^2 \Delta$. From mean values of $D'^2 \Delta$, the signal deflections are

Table IIa.

Calibration observations for RCA 931-A photometer.

Photomultiplier voltage :- - 950 v. D = 78.9 cms.

Power supply for amplifier :- + 250 v.

Amplifier filaments :- 6.1 v.

Neutral filter used :- ON 321.

	Distance D' in cm.	Deflection (μA) caused for filters 5300A	5577A	$D'^2 \Delta$ for 5300A	5577A
	(Current in the lamp 2.725 Amps.)				
1.	170.3	235	500	8.305 · 10^6	1.450 · 10^7
2.	152.4	350	605	8.303	1.406
3.	136.5	420	765	7.924	1.425
4.	121.3	535	920	7.870	1.353
			Mean	8.030 · 10^6	1.409 · 10^7
**	200	209	352		
	(Current in the lamp 2.020 Amps.)				
1.	249.5	213	390	1.275 · 10^7	2.253 · 10^7
2.	218.7	235	500	1.299	2.032
3.	190.9	330	655	1.403	2.302
4.	161.3	525	915	1.386	2.321
			Mean	1.337 · 10^7	2.315 · 10^7
**	200	339	570		

Table IIb(1)

Calibration observations for EMI 6095 photometer.

Photomultiplier voltage :- -1100 V. D = 93.5 cm.

Power supply for amplifier :- + 250 v.

Amplifier filaments :- 6.3 v.

Neutral filter used :- OY 321 + OY 3211.

	Distance D' in cm.	Deflection (μA) caused for filters 5300A	5577A	$D'^2 \Delta$ for 5300A	5577A
	(Current in the lamp 2.735 Amps.)				
1.	219.7	330	390	$1.719 \cdot 10^7$	$1.719 \cdot 10^7$
2.	177.1	520	530	1.631	1.631
3.	151.3	685	685	1.568	1.569
4.	133.5	800	790	1.490	1.472
			Mean	$1.602 \cdot 10^7$	$1.599 \cdot 10^7$
* * *	200	400	400		
	(Current in the lamp 2.935 Amps.)				
1.	224.0	460	455	$2.309 \cdot 10^7$	$2.283 \cdot 10^7$
2.	200.4	555	560	2.229	2.249
3.	170.3	730	770	2.269	2.233
4.	151.4	900	930	2.146	2.133
			Mean	$2.240 \cdot 10^7$	$2.229 \cdot 10^7$
* * *	200	532	558		

Table IIb(ii)

Calibration observations for EMI 6095 photometer.

Neutral filter used :- OY 321 + OY 3211 + OY 32111.

	Distance D' in cm.	Deflection (μA) caused for filters 5893A	6300A	$D'^2\Delta$ for 5893A	6300A
	(Current in the lamp 2.325 Amps.)				
1.	197.9	410	295	$1.306 \cdot 10^7$	$1.155 \cdot 10^7$
2.	165.9	570	410	1.369	1.129
3.	145.9	695	500	1.430	1.065
4.	131.0	865	620	1.434	1.064
			Mean	$1.385 \cdot 10^7$	$1.103 \cdot 10^7$
∴	200	305	219		
	(Current in the lamp 2.725 Amps.)				
1.	152.3	535	385	$1.241 \cdot 10^7$	$0.893 \cdot 10^7$
2.	133.4	695	475	1.184	0.846
3.	116.7	920	590	1.117	0.804
4.	103.2	910	670	1.029	0.753
			Mean	$1.142 \cdot 10^7$	$0.825 \cdot 10^7$
∴	200	227	164		

calculated for D' = 200 cms. These also are included in the tables.

(d) The derivation of the formula

The aim in deriving the formula is to calculate the effective surface brightness B of the screen in unit mega quanta cm^{-2} sec^{-1} $sterad^{-1}$, which causes unit deflection on the recorder. This can be converted to Rayleigh by the simple relation $R = 4\pi B$.

The procedure would be to calculate the effective energy radiated by the screen (cm^{-2} sec^{-1} $sterad^{-1}$) corresponding to unit deflection on the photometer. This energy of the continuous spectrum band is compared with the equivalent energy from a monochromatic source to estimate the surface brightness B of the sky. Finally B is converted to Rayleighs.

Starting from the source end (refer Fig.10) the spectral energy distribution of the tungsten filament, according to Planck's radiation law would be

$$J_\lambda \, d\lambda = c_1 \, e^{-c_2/\lambda T} \, \lambda^{-5} d\lambda \quad \text{ergs cm}^{-2} \text{ sec}^{-1}.$$

where c_1 is the 1st radiation constant,

c_2 = 2nd radiation constant,

λ = the wavelength under consideration,

$d\lambda$ = the wavelength interval chosen,

J_λ = the energy radiated at wavelength λ,

T = the colour temperature of the filament in °K.

c_1 = $3.74 \cdot 10^{-5}$ ergs cm^{-2} sec^{-1}.

c_2 = 1.438 cm. deg.

Taking into account the area of the filament used for illumination and the transmission coefficient of its envelope, the energy radiated from the filament would be $0.9\ J_\lambda\, d\lambda\, A$ ergs sec^{-1}.

The energy in a unit solid angle perpendicular to the plane of the filament would be

$$\frac{0.9\ J_\lambda\, d\lambda\, A}{\pi} \text{ ergs sec}^{-1} \text{ sterad}^{-1}.$$

The illumination by this source on the screen at a distance D' from the filament and inclined at an angle θ would be

$$\frac{0.9\ J_\lambda\, d\lambda\, A \cos\theta}{\pi\ D'^2} \text{ ergs cm}^{-2} \text{ sec}^{-1}.$$

The screen with the diffusion coefficient 0.075 would radiate the energy

$$\frac{0.9 \cdot 0.075\ J_\lambda\, d\lambda\, A \cos\theta}{\pi^2\ D'^2} \text{ ergs cm}^{-2} \text{ sec}^{-1} \text{ sterad}^{-1}.$$

Now the dependence of the transmission of the filters and the response of the photomultiplier upon wavelength should be considered. The energy at wavelength λ in the interval $d\lambda$ would then be

$$\frac{0.9 \times 0.075\, J_{\lambda}\, d\lambda\, A \cos\theta\, t_{\lambda}\, T_{\lambda}\, R_{\lambda}}{\pi^2 D'^2}$$ ergs cm^{-2} sec^{-1} sterad^{-1} of the screen,

where t_{λ} is transmission of the interference filter at wavelength λ.

T_{λ} = transmission of neutral filter at λ.

R_{λ} = relative response of the photomultiplier at λ.

The integration of the above expression in the interval λ_1 to λ_2 would give the effective energy in ergs cm^{-2} sec^{-1} sterad^{-1} of the screen causing a deflection Δ on the recorder. Hence, the energy per unit deflection would be

$$\frac{0.9 \times 0.075\, A \cos\theta \int_{\lambda_1}^{\lambda_2} J_{\lambda}\, t_{\lambda}\, T_{\lambda}\, R_{\lambda}\, d\lambda}{\pi^2 D'^2 \Delta} = E_1 \quad \text{(say)} \quad .. \quad (1)$$

For a monochromatic source the equivalent energy in mega quanta would be

$$E_2 = n \times 10^{+6}\, h\nu\, T_{em}\, R_{em}\, W \quad .. \quad .. \quad .. \quad .. \quad .. \quad (2)$$

where T_{em} is filter transmission at emission wavelength,

R_{em} = photomultiplier response at emission wavelength,

W = equivalent bandwidth.

Equating (1) and (2) $E_1 = E_2$ or

$$n = \frac{E_1 \lambda \times 10^{-6}}{hc\, T_{em} R_{em} W} \text{ megaquanta cm}^{-2}\text{ sec}^{-1}\text{ sterad}^{-1} \quad .. \quad .. \quad (3)$$

which is the surface brightness B of the screen.

$$\text{Now } R = 4\pi B$$

$$= 4\pi n$$

$$= \frac{4\pi E_1 \lambda \cdot 10^{-8}}{hc\, T_{cm} R_{cm} W} \quad \dots \quad \dots \quad \dots \quad \dots \qquad (4)$$

substituting E_1 from (2) in (4) we get

$$R/uA = \frac{4 \cdot 0.9 \cdot 0.078 \cdot 10^{-8}\, A \cos\theta\, \lambda\, c_1 \int_{\lambda_1}^{\lambda_2} e^{-c_2/\lambda T} \lambda^{-5} t_\lambda T_\lambda R_\lambda\, d\lambda}{\pi hc\, T_{cm} R_{cm} W\, D'^2 \Delta}$$

with $\cos\theta = 0.9951$ and

$D' = 200$ cm (with λ in cm),

$A = 0.0123\ cm^2$

$$R/uA = \frac{6.503 \cdot 10^{-9}\, \lambda\, S}{T_{cm} R_{cm} W \Delta} \quad \dots \quad \dots \quad \dots \quad \dots \quad \dots \qquad (5)$$

where $S = \int_{\lambda_1}^{\lambda_2} e^{-c_2/\lambda T} \lambda^{-5} t_\lambda T_\lambda R_\lambda\, d\lambda$, and λ now expressed in Angstroms.

S is evaluated by numerical integration.

W is defined as $W = \dfrac{\int_{\lambda_1}^{\lambda_2} t_\lambda R_\lambda\, d\lambda}{T_{cm} R_{cm}}$.

The quantities involved in the above derivation are presented in table III.

Roach[8] and Furuhata have brought to notice that the laboratory calibration and stellar calibration are not identical, but are related to each other as : stellar C/I = 1.25 laboratory C/I, which they had derived empirically. Therefore the last row of table III was obtained by multiplying the laboratory calibration by a factor 1.25.

The RCA 931-A photometer was calibrated against Roach's travelling photometer in May 1958. This yielded an empirical relation

$$R_{5577} = 0.37\ (d_{5577} - 65) \quad \text{.. .. ..} \quad (a)$$

where R_{5577} is the intensity in Rayleighs corrected for the background and d_{5577} is the deflection caused by the signal for the 5577 Å filter.

It can be seen that the calibration factor 0.37 of (a) agrees fairly well with the corresponding value 0.40 of the last row of table III.

The factors in the last row of table III were used for converting the readings in arbitrary units (µA deflections) to Rayleighs.

10. Contamination due to background and its elimination

The interference filters which are used to select the appropriate emissions under study transmit along with these emissions, the continuous background radiation, the light of the astronomical origin and also some unwanted radiations. All these radiations contaminate the observations.

For eliminating the background radiation, it is assumed that the spectral energy distribution of the background is that of a G2 star. With this assumption the background is estimated by employing a 5300 A filter. The energy transmitted by this filter is removed from the total energy transmitted by the filter used for selecting the emission, with appropriate correction for filter transmission etc. As the background radiation in the direction of the celestial pole was found to remain fairly steady the following relations were used for eliminating the background.

$$R_{5577} = 2.37\ (d_{5577} - 65) \quad .. \quad .. \quad .. \quad .. \quad .. \qquad (a)$$

as obtained from the calibration with Roach's[4] photometer.

$$R_{5893} = 0.73\ d_{5893} - 115 \quad .. \quad .. \quad .. \quad .. \quad .. \qquad (b)$$

$$R_{6300} = 1.33\ d_{6300} - 116 \quad .. \quad .. \quad .. \quad .. \quad .. \qquad (c)$$

where R's give intensity in Rayleighs corrected for the background and d's represent the deflections produced by signal on the recorder.

In addition to the background, 5300 A filter transmits the weak bands of OH (6-0 and 9-2). The 5577 A allows the weak band (7-1) of OH. The 5893 A and 6300 A filters transmit the strong OH bands (7-2) and (9-3) respectively. No correction was made for the effect of the contamination due to OH bands.

The observations are summarised in the next chapter.

REFERENCES

1. Elmore W.C. and Sands M. 1949 Electronic Experimental Techniques, McGraw-Hill Book Co.

2. Hunten D.M., Roach F.E. and Chamberlain J.W. 1956 J.Atmos.Terr.Phys., 8, 345.

3. Roach F.E. 1957 Annales of I.G.Y., 4, 115.

4. Roach F.E. 1958 N.B.S.Report, 5501.

Table III

Calibration of airglow photometers.

Filter No.	I	II	III	IV	V	VI
The radiation under study	5300A background	5577A OI green line	5300A background	5577A OI green line	5893A Na-D lines	6300A OI red lines
Photomultiplier used	— RCA 931-A —		— EMI 6095 —			
Photomultiplier response R_{em} at emission λ.	0.50	0.323	0.82	0.69	0.516	0.27
Equivalent bandwidth W of the filter in A	91.2	135.3	152.4	79.5	150.3	139.7
Transmission of filter T_{em} at emission λ.	0.19	0.18	0.122	0.21	0.255	0.287
Inclination of the lamp with the screen	— $9^{\circ}.9$ —					
S for (a) 2075°K	$8.295 \cdot 10^{7}$	$1.214 \cdot 10^{8}$	$7.150 \cdot 10^{7}$	$7.650 \cdot 10^{7}$	$6.804 \cdot 10^{7}$	$4.709 \cdot 10^{7}$
(b) 2155°K (for RCA 931-A) 2115°K (for EMI 6095)	$1.342 \cdot 10^{8}$	$1.920 \cdot 10^{8}$	$9.013 \cdot 10^{7}$	$9.635 \cdot 10^{7}$	$8.990 \cdot 10^{7}$	$5.812 \cdot 10^{7}$
Deflection on Avo 8 for (a)	202	352	400	400	286	206
μA (D' = 200 cm) (b)	332	579	562	556	384	276
Deflection (μA) on recorder (a)	160	279	317	317	227	164
Δ (b)	264	460	446	441	305	219
∴ S/Δ (a)	$5.184 \cdot 10^{5}$	$4.351 \cdot 10^{5}$	$2.257 \cdot 10^{5}$	$2.413 \cdot 10^{5}$	$2.997 \cdot 10^{5}$	$2.871 \cdot 10^{5}$
(b)	$5.084 \cdot 10^{5}$	$4.174 \cdot 10^{5}$	$2.021 \cdot 10^{5}$	$2.184 \cdot 10^{5}$	$2.948 \cdot 10^{5}$	$2.654 \cdot 10^{5}$
∴ S/Δ (mean)	$5.134 \cdot 10^{5}$	$4.263 \cdot 10^{5}$	$2.139 \cdot 10^{5}$	$2.229 \cdot 10^{5}$	$2.973 \cdot 10^{5}$	$2.763 \cdot 10^{5}$
Constant term	— $6.596 \cdot 10^{-9}$ —					
Rayleighs / μA (Laboratory method)	2.100	1.992	0.491	0.734	0.583	1.061
Rayleighs / μA (Astronomical) ($R_{lab} \cdot 1.25$)	2.625	2.490	0.614	0.918	0.729	1.326

CHAPTER III

SUMMARY OF OBSERVATIONS ON AIRGLOW

CONTENTS

CHAPTER III

SUMMARY OF OBSERVATIONS ON AIRGLOW

1. Introduction

The observations of the OI green line 5577 A and the background radiation in the region near 5300 A were taken with a polar photometer using an RCA 931-A photomultiplier. For OI red lines 6300-6364 A and Na-D lines 5890-5896 A, an alt-azimuth airglow photometer, with an EMI 6095 photomultiplier was used. All the intensities were recorded towards the pole, on clear nights when there was no moon.

Tables I(a) and I(b) give the number of observations in each month during the period of operation for the emissions (a) OI green line and (b) OI red lines and Na-D lines.

For obtaining the additional information full sky scanning observations were taken for 13 nights from November 1959 to April 1960. These will be discussed in a separate chapter.

2. Diurnal variation

For studying the variations of intensity during the night, the data from October 1957 to December 1959 were grouped according to seasons : (a) Autumn - October and

Table I(a)

Number of nights of observations in each month for 5577 A.

Month	1935-36	1936-37	Year 1937-38	1938-39	1939-40	Total
			Number of observations			
Oct.	-	-	3	8	6	17
Nov.	3	-	4	14	11	32
Dec.	8	-	17	13	11	49
Jan.	7	7	18	14	17	63
Feb.	10	11	17	14	2	54
Mar.	8	9	19	17		53
Apr.	2	11	16	15		44
May	2	11	17	10		40
Jun.	-	-	9	-		9
					Total	361

Table I(b)

Number of observations in each month for 5893 and 6300 A.

Oct.	5	-	8	13
Nov.	4	14	11	29
Dec.	-	3	13	16
Jan.	13	10	16	39
Feb.	5	14	2	21
Mar.	13	17		30
Apr.	-	15		15
May	6	10		16
			Total nights	179

November, (b) Winter - December to February, and (c) Spring - March to May. In the monsoon months from June to September, the data are unfortunately lacking owing to cloud and rain.

(a) OI green line

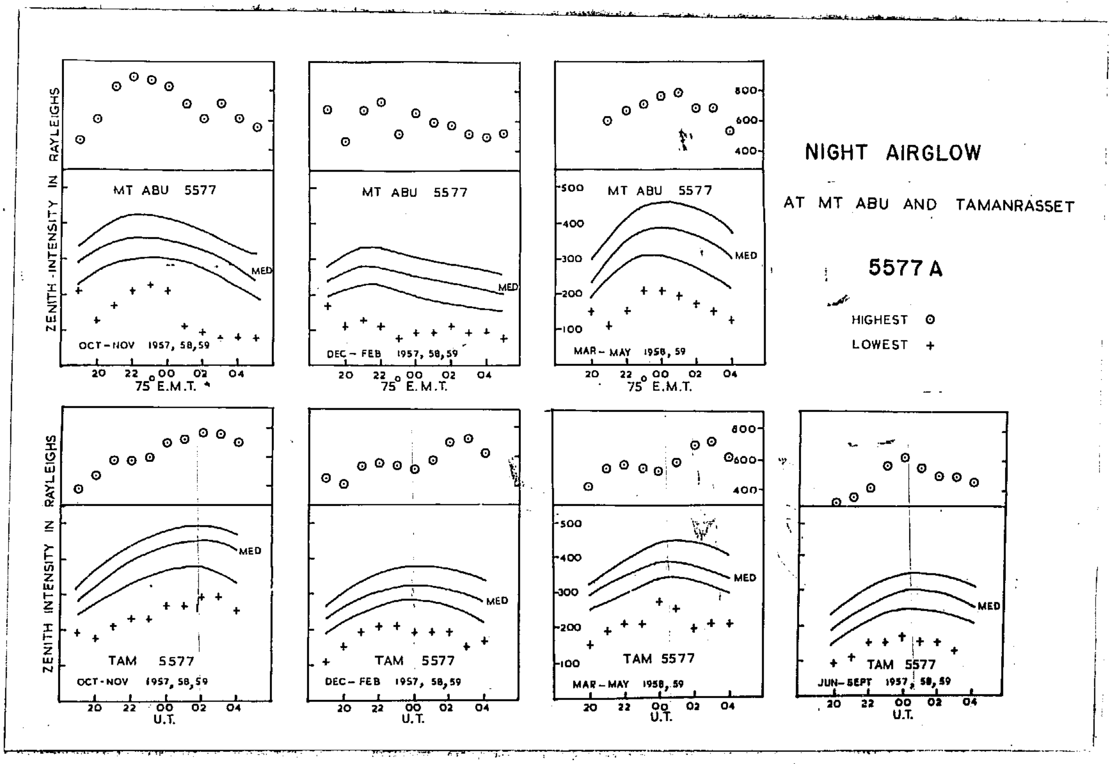

Fig.1(a). Nocturnal variation of 5577 A airglow at Mt.Abu and at Tamanrasset in different seasons.

Fig.1(a) shows the nocturnal variations of 5577 A in each of these seasons. The maximum and minimum intensities are shown by ⊙ and + respectively. The curves in each group represent the upper, the middle and the lower quartiles respectively i.e. boundaries above which 25, 50, 75 percent observations lie. All the groups show an increase in intensity during the first part of the night. The intensity reaches a maximum generally before midnight and is followed by a fall towards the early morning.

The maximum in autumn occurs at about 22 hours local time, in winter at 21 hours and in spring at about 0 hour. The hour of maximum intensity thus changes from season to season. The median intensities were 350 Rayleighs in autumn, 220 R in winter and 300 R in spring. The nocturnal variation was maximum in spring.

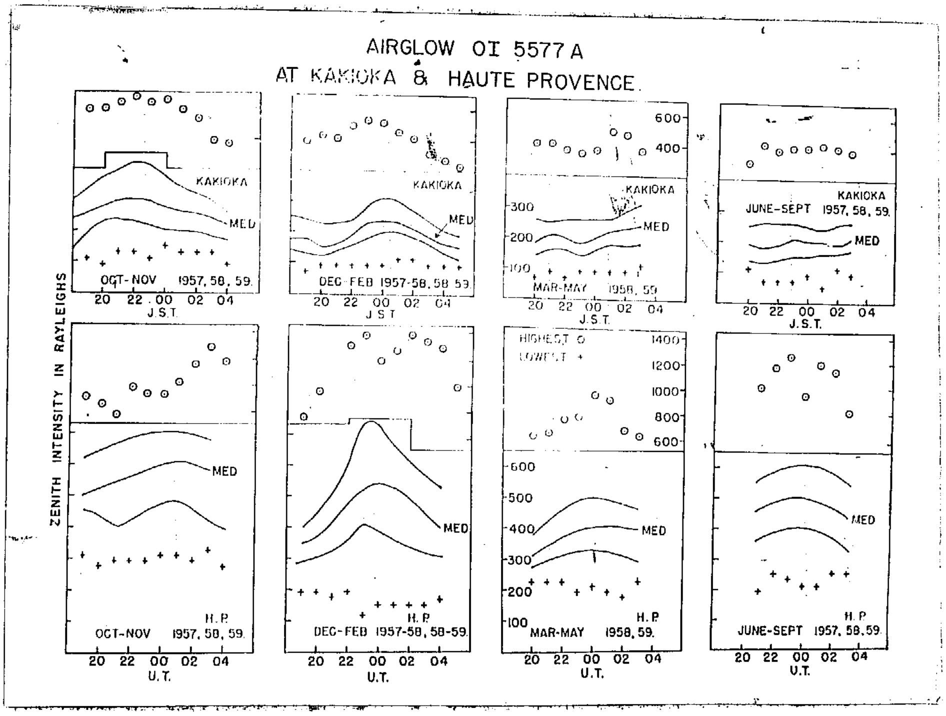

Fig.1(b). Nocturnal variation of OI green line of airglow at Kakioka and at Haute Provence.

In Figs.1(a) and 1(b), the nocturnal variations at

Tamanrasset, Kakioka and at Haute Provence, over the same period are shown for the sake of comparison. The geographic coordinates and the time of occurrence of maximum for these stations are summarised in table II.

<u>Table II.</u>

Station	Latitude	Longitude	Local time for max. (hrs.)	Mean Zenith Intensity (Rayleighs)
Mt.Abu	24°.6N	72°.7E	21 to 00	350
Tamanrasset	22°.8N	5°.5E	00 to 02	390
Kakioka	36°.2N	140°.2E	22 to 00	250
Haute Provence	43°.9N	5°.7E	23 to 00	505

(Averaged over the period October to May 1957-58, 1958-59.)

The station Tamanrasset, which has the same geographic latitude as that of Abu but a difference in longitude of 70°, exhibits variations of intensity, which are quite comparable with those occuring at Abu in the corresponding seasons. The hour of the occurrence of the maximum also changes from season to season, and it is interesting to find that the maximum at Tamanrasset occurs usually after midnight.

The high latitude station Haute Provence has intensities much higher than those at Abu and Tamanrasset, in all the seasons. At Haute Provence the maximum occurs at about local midnight, and the nocturnal variation is prominent in winter.

Kakioka, the Japanese station having moderate latitude observes the maximum intensity between 22 to 01 local hours. The nocturnal variations dominate autumn and winter but are practically absent in spring and summer. Kakioka which lies between Haute Provence and Abu has airglow weaker than at the two stations. This can also be seen by referring to the average airglow intensities presented in table II.

The other Indian station Poona[1], observes a maximum of intensity a little before local midnight.

Rayleigh[2] (1928) observed a midnight maximum in England for the OI green line. From the observations at Haute Provence and Cactus Peak Roach, Williams and Pettit[3] concluded that the OI green line exhibits a maximum one hour after midnight.

Thus all the stations observe the maximum of intensity around local midnight though the time of occurrence varies with place and season.

(b) <u>OI red lines 6300-6364 Å.</u>

The diurnal variations at two stations Mt.Abu and Haute Provence for different seasons are shown in Fig.2.

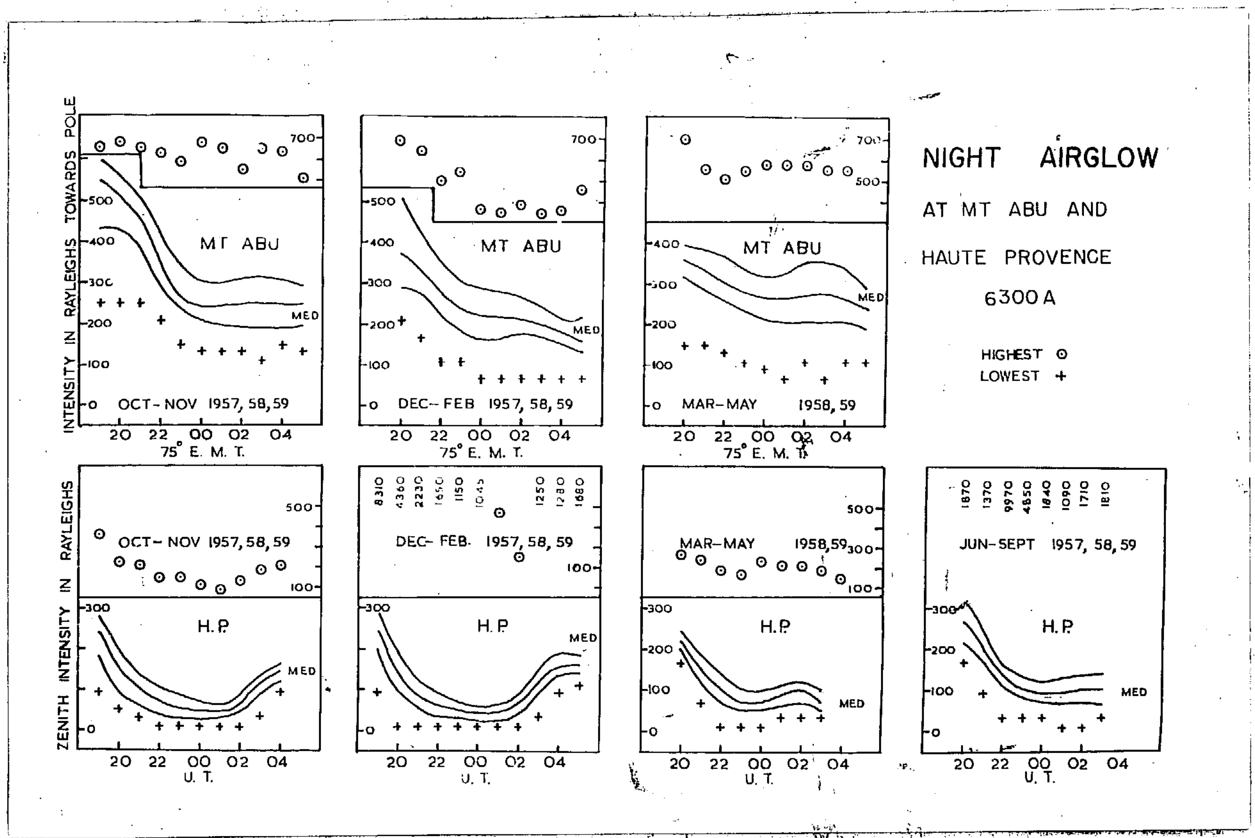

Fig.2. Nocturnal variation of the OI red lines at Mt.Abu and at Haute Provence.

At Mt.Abu the intensity of the OI red line shows a rapid decrease upto local midnight, and remains uniformly steady afterwards. This post-crepuscular effect is quite prominent in autumn and less so in spring.

At Haute Provence the highest intensities usually shown by ⊙ are much stronger in winter and summer. This is due to auroral activity. At Haute Provence, the intensity also decreases rapidly upto midnight similar to what is observed at Abu, but later it increases towards dawn. The increase in intensity during the early hours of morning is pronounced in autumn and winter and practically absent in spring and summer.

It should be mentioned that Roach[4] (1954) and Barbier[5] (1950) have observed the post-crepuscular effect of the OI red lines, with intensity decreasing rapidly in the first four hours of the night and later remaining more or less steady for a few hours. In their latitude they find another rise of intensity in the pre-dawn hours which is well correlated with magnetic activity. Barbier has stated that the post-crepuscular effect was strong in November and absent in summer.

(c) <u>Na-D Lines</u>

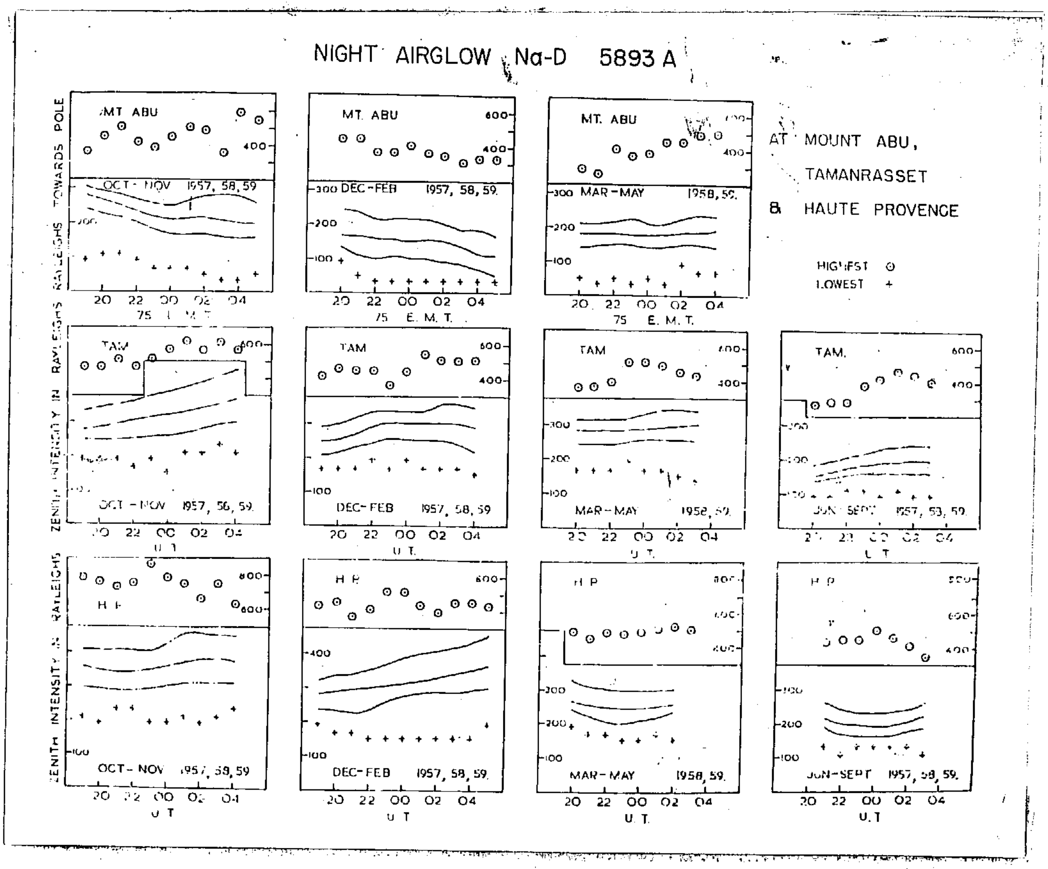

Fig.8. Nocturnal variation of Na-D lines at Mt.Abu, Tamanrasset and at Haute Provence.

Fig.3 represents the nocturnal variations for the Na-D lines at the stations Abu, Tamanrasset and Haute Provence for different seasons.

At Abu the intensity slightly decreases from late evening towards dawn in autumn and winter. The nocturnal variation is practically absent in spring.

At Tamanrasset and Haute Provence the intensity of the sodium lines slowly increases towards dawn during all the seasons. But the increase in intensity is appreciable in autumn at Tamanrasset and in winter at Haute Provence. The intensities at Tamanrasset and Haute Provence are quite comparable in corresponding seasons and are much higher than those at Abu.

It should however be noted that Roach (1954) did not observe any diurnal variation for the Na-D lines. Pettit and Manring[3] (1955) did observe a tendency for a relatively fainter start during the first hours of the night with a slight rise towards dawn.

3. Seasonal variation

For studying the seasonal variations, the data of all nights on which observations at 23, 00, 01 hours local time were available, were used. The monthly mean intensities were computed from these data. For comparing the seasonal variations at Abu with those occuring at other stations, the intensities at pole for 5577, 6300 and 5893 A were divided by 2.0, 1.4 and 1.7 respectively.

(a) OI green line

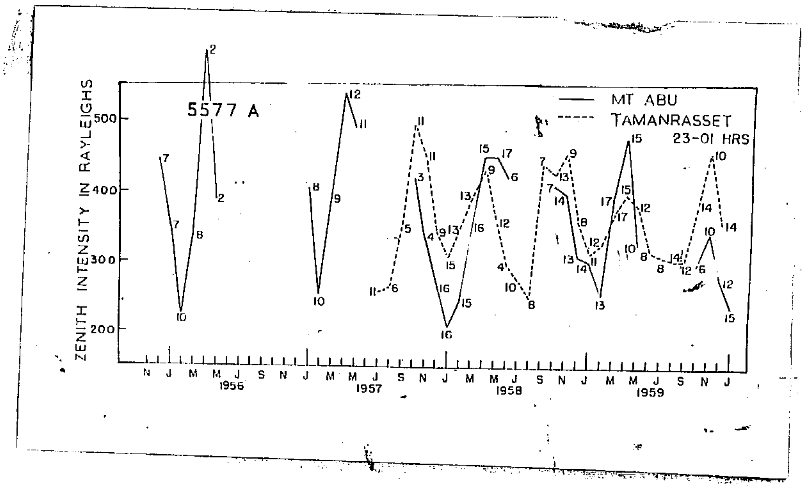

Fig.4(a). Seasonal variation of airglow 5577 A at Mt.Abu and Tamanrasset.

The monthly mean intensities at Abu, obtained by the above procedure are shown in Fig.4(a). The figures in the graph represent the number of observations available in the respective months. The airglow show a minimum in January-February and a maximum in April. In Figs.4(a) and (b) are shown the seasonal variations (treated in the same way) at Tamanrasset, Kakioka and Haute Provence, during the I.G.Y. and the I.G.C. period. The seasonal variations at Abu and Tamanrasset are quite similar in character. Tamanrasset observations show another minimum in June to September.

The Japanese station Kakioka observes maxima in October-November and May-June and minima in March-April and July-August.

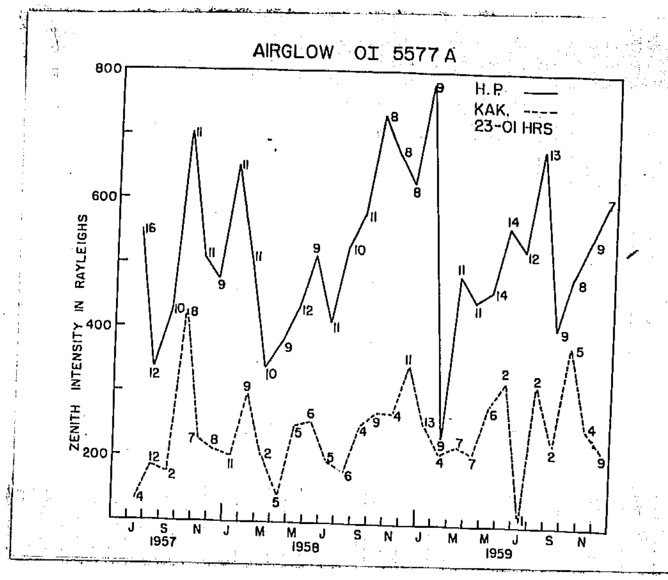

Fig.4(b). Seasonal variation of airglow 5577 Å at Kakioka and at Haute Provence.

The high latitude station Haute Provence has maximum intensity from October to January with a small dip in December, and the intensity reaches a minimum in February.

The intensities at Haute Provence are quite high. At the Japanese station Kakioka the airglow is in general weak.

It is interesting to find that all the stations have one maximum of intensity in October-November, whereas the phases of other maxima and also of the minima do not coincide.

From Figs.4(a) and (b), it can be concluded that the OI green line shows in the subtropical regions, two maxima during the year in the two equinoctial seasons and minima in winter and summer.

Rayleigh[6] (1928) observed a maximum for OI green line in autumn and a minimum in early spring for the observations in England. For the moderate latitude station Cactus Peak, Roach[7] (1955) observes a maximum in September and a minimum in March and December. Barbier[8] (1958) noticed four well established maxima for the OI green line at Haute Provence.

(b) OI red lines

The seasonal variations in the intensity of the OI red lines are shown in Fig.5, for the stations Abu, Tamanrasset and Haute Provence. At Abu OI 6300 shows a minimum in winter similar to that observed at Haute Provence. On the other hand the seasonal variations at Tamanrasset are quite different although it is at the same latitude as Abu.

Tamanrasset observes maximum intensity in November and minimum in June. Also the large amplitude changes in the seasonal variations at Tamanrasset should be noted. At Haute Provence the OI red lines are much weaker than those at Tamanrasset. It has a summer maximum and a winter minimum.

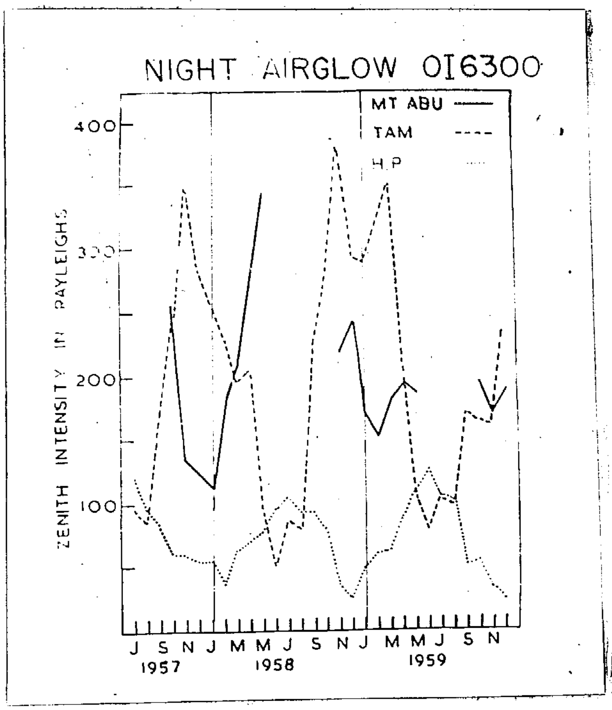

Fig.3. Seasonal variation of the red airglow at Abu, Tamanrasset, and Haute Provence.

Roach (1954) observed a winter minimum for the OI red lines at Cactus Peak. For the Haute Provence observations Barbier (1955) noticed a maximum in November and a minimum in July.

For studying the seasonal variation of the post-crepuscular effect of the OI red lines, the monthly mean intensities were obtained for the earlier hours 20, 21, 22 local time. The deviations were obtained from the mean midnight values (which refer to 23, 00, 01 hours). The deviations were divided by the respective monthly means. These normalised values of the deviations for the same three stations are presented in Fig.6. It can be seen that at Tamanrasset the post-crepuscular effect is negligible. Abu and Haute Provence observe the post-crepuscular effect which is very prominent in October-November and becomes less important in summer.

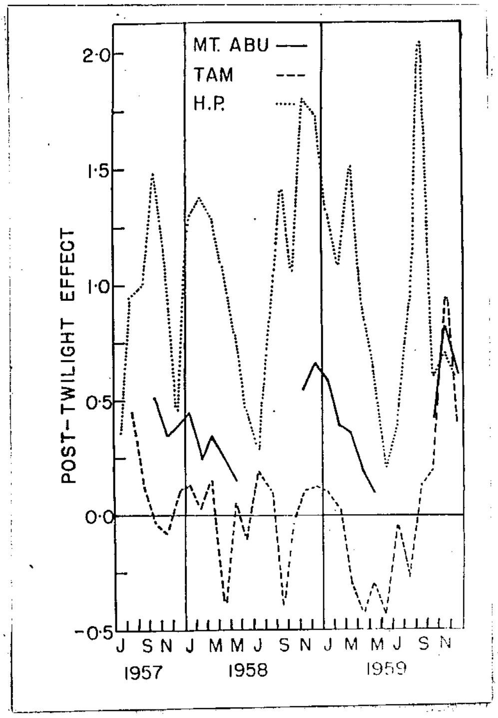

Fig.6. Seasonal variation of the post-crepuscular effect for OI red lines at Abu, Tamanrasset and Haute Provence.

(c) <u>Na-D lines</u>

Fig.7 represents the seasonal variation for Na-D lines at these stations. It is interesting to see that the seasonal variations at Tamanrasset and Haute Provence are very much similar in character. They show a maximum in November and a minimum in June-July. The intensity at Abu is much small as compared with that observed at these stations and its seasonal variations are quite different, the reason for which is not well understood. Abu observes a minimum in winter.

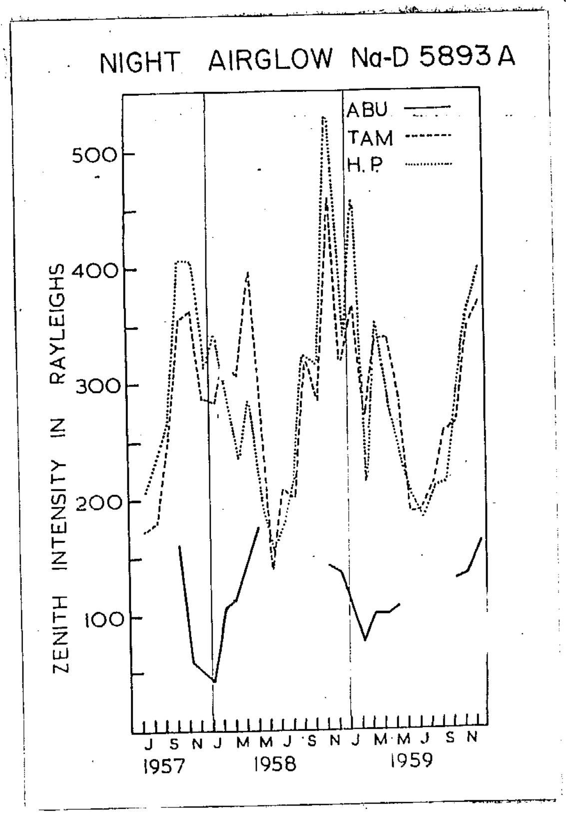

Fig.7. Seasonal variation of Na-D lines at Abu, Tamanrasset and Haute Provence.

Roach (1954) observes a minimum in winter for Na-D lines at Cactus Peak, whereas Barbier (1955) notices a maximum in November and a minimum in July for observations at Haute Provence.

4. The isopleth map for airglow 5577 Å (Mt.Abu)

The diurnal and the seasonal variations of the zenith sky intensity of the OI green line at Abu from October 1958 to May 1959 are shown in a composite way by means of an isopleth map in Fig.3. The highest and the lowest intensities are shown by X and N respectively. The contours represent the hour of the night and the month of the season having the same intensity. In February the intensity is the lowest. There are two maxima, one in October and another in April. The large nocturnal variations with a broad midnight maximum in April should be noted.

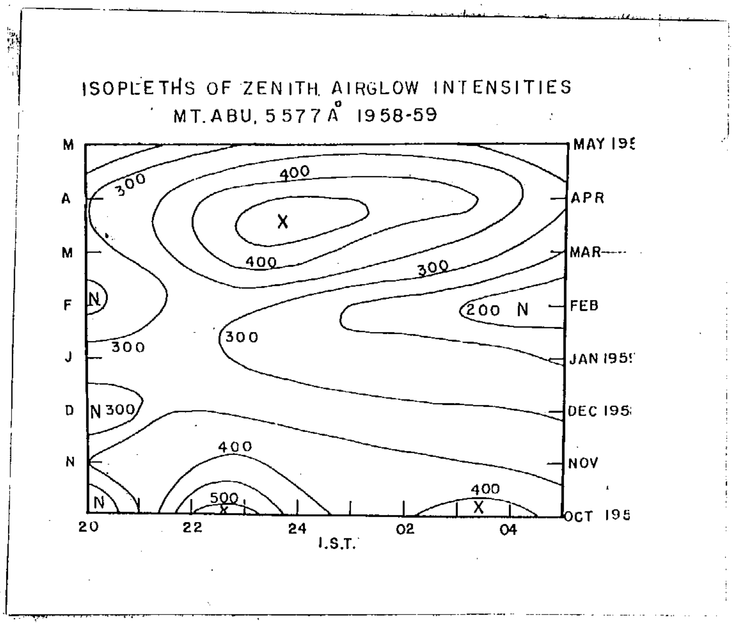

Fig.3. Isopleth map of the OI green line over the period October 1958 to May 1959.

REFERENCES

1. Chiplonkar M.W. and Kulkarni P.V. 1950 Indian J.Met.& Geophys., 2, 133.

2. Rayleigh L. 1921 Proc.Roy.Soc., 112, 11.

3. Roach F.E., Williams D.R. and Pettit H.B. 1953 J.Geophys.Res., 58, 73.

4. Roach F.E. 1954 Proc.National Acad.Sci., 40, 950.

5. Barbier D. 1955 The airglow and the aurorae, Pergamon Press, p.38.

6. Pettit H.B. and Manring E.R. 1955 Ann de Geophys., 11, 377.

7. Roach F.E. 1955 Ann de Geophys., 11, 214.

8. Barbier D. 1956 Vistas in Astronomy, V.2, Pergamon Press, p.920.

CHAPTER IV

VARIATIONS OF INTENSITY OF 5577 A OVER THE SKY.

CONTENTS

CHAPTER IV

VARIATIONS OF INTENSITY OF 5577 A OVER THE SKY

A - HEIGHT OF THE EMISSION LAYER

1. Introduction

The observations towards the pole are useful for the study of diurnal and seasonal variations of airglow and their relationship with other geophysical phenomena such as the solar activity, magnetic activity etc.

Problems like the variability of airglow over the sky or determination of the height of the emitting layer, require observations all over the sky.

For this purpose, an alt-azimuth scanning photometer (Fig.1(b), Chapter II) using an EMI 6095 photomultiplier as the sensing element was used to scan the sky manually.

It would be preferable to have an automatic arrangement to scan the whole sky at different altitudes and azimuths, but with the limited resources available, it was only possible to construct a meridian scanning photometer. The detailed working of the instrument and samples of its records are presented in a separate paper.

2. Method of observation

The photometer was kept in a corner of an open terrace of a building situated on a small hill at Mt.Abu. The observation site was free from the effects of city light. Half an hour before the commencement of the observation the electronic unit was switched on for warming the equipment. Deflections were read on an Avo 8 meter.

The use of an appropriate optical filter allowed the selection of the OI green line.

The sky was scanned in a series of almucantars in the following way. The photometer was turned to 40° zenith distance, and readings were taken for every 22½° of the azimuth, beginning from the north in a N-W-S-E cycle. Similar observations were taken for the zenith distances 60°, 70°, 75° and 80°. Zenith readings were taken both at the beginning and end of the observations in other directions. The observations with the 5577 A filter were followed by those with the 5300 A filter in a similar way, for estimating the background radiation. The total time needed for one set i.e. observations with both the filters, was approximately 10 minutes. Thus all the observations of a set do not form a snapshot of the sky but are somewhat staggered in time. It was assumed that the intensity pattern over the sky did not change appreciably during the period of observation.

The number of observations that could be made with each filter is 10 x 8 + 1 = 81, but as the building obstructed one quadrant of the sky, the number of observations were reduced to 67. About 10 sets of observations were obtained on each night from late evening to predawn.

The number of sets available and the sky conditions during the period of operation are summarised in table I.

Table I.

Summary of observations over the sky.

Sr. No.	Date	No. of sets available.	Sky condition
1	9-10 Nov.58	8	Clear
2	10-11	10	"
3	11-12	10	"
4	8-9 Jan.59	10	Slight haze
5	9-10	10	Clear
6	11-12	7	Cloudy at S horizon at 0400 hrs.
7	6-7 Feb.59	10	Clear
8	7-8	10	Clear
9	8-9	10	"
10	7-8 Mar.59	10	"
11	8-9	10	"
12	9-10	6	Cloudy at W horizon at 0300 hrs.
13	5-6 Apr.59	9	Clear
14	7-8	10	"
15	8-9	10	"
15 Nights		140 sets	

Fig.1 shows the variation of intensity observed for the 5577 and 5300 A filters. It should be noted that the intensity for 5577 A is minimum at zenith, increases with increasing zenith distance and passes through a maximum. Even though the radiation from the upper atmosphere in the 5300 A region was small, the 5300 A filter showed an appreciable deflection, due to the background radiation.

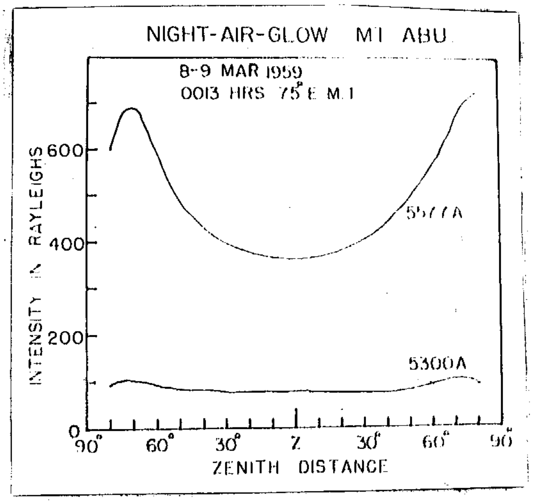

Fig.1. Variation of airglow 5577 and 5300 A with zenith distance.

3. The determination of the height of the emitting layer

(a) General considerations involved in Van Rhijn technique

For determining the height of the emitting layer from the observations all over the sky, the Van Rhijn technique was used.

According to Van Rhijn formula

$$\frac{I_z}{I_0} = V_z = \left[1 - \frac{R^2}{(R + h)^2} \sin^2 z\right]^{-\frac{1}{2}} \quad \ldots \quad \ldots \qquad (1)$$

or

$$h = R \left[\frac{V_z \sin z}{\sqrt{(V_z^2 - 1)}} - 1\right] \quad \ldots \quad \ldots \quad \ldots \qquad (2)$$

where

I_z - is the intensity at zenith angle z,

I_0 - intensity at zenith,

R - radius of the earth,

h - height of the emitting layer from the surface of the earth,

z - the inclination of the path of the incoming ray away from zenith.

The formula has been derived under following assumptions :-

(1) The thickness of the layer is small compared to the radius of the earth.

(2) The layer is at a constant height from the surface of the earth.

(3) It possesses uniform intrinsic brightness all over.

(4) The lower atmosphere which would otherwise affect the results is absent.

Careful consideration shows that none of the assumptions can be rigorously true.

All these assumptions have been studied in detail by Elvey and Farnsworth[1], Barbier[2], Roach et al[3] and Ashburn[4].

The method is unable to yield the thickness of the layer, but it refers to its average height. The inclination of the layer with the surface of the earth does not introduce any serious systematic error in the height deductions. The airglow is known to exhibit a patchy nature, but the average height can be obtained by using a large bulk of data.

The radiation emitted by the layer is affected by the lower atmosphere in two ways. Due to self-absorption, the lower atmosphere offers partial opacity to the radiation, thus causing attenuation. There is also scattering of the radiation by the gaseous matter of the lower atmosphere. The effect of scattering is to increase slightly, the intensity observed along the line of sight. There is further attenuation due to the presence of haze or dust.

In addition, the effect of reflection from the earth's surface, known as the effect of albedo, has to be taken into account.

The observed intensity does not increase with increasing zenith distance as expected by the Van Rhijn formula, but actually decreases near the horizon after passing through a maximum at a zenith distance between 70°

to 35° depending on the height of the emitting layer. This is due to atmospheric extinction. The effect of scattering is to increase the observed intensity with increasing zenith distance.

In addition to the assumptions involved in the derivation of the Van Rhijn formula, the inherent errors due to observing instruments have to be taken into account.

The photometer with an optical interference filter acts as a wide slit spectrograph. The 5577 A filter transmits the background radiation of astronomical origin and also the weak (7-1) band of OH. The effect due to this contamination has to be taken into account.

The elimination of the effect of contamination leads to two methods. These are known as (1) two colour method and (2) single colour method. The methods have been considered in great detail by Roach[5] and Roach and Meinel[3].

In the two colour method, the background radiation in the spectral region under study is assumed to be that due to a G_0 star, and is estimated by a 5300 A filter. The 5300 A filter is known to transmit the weak bands (6-0) and (9-3) of OH, whereas 5577 A filter transmits (7-1) band of OH. It is however assumed that the intensities of OH bands transmitted by both the filters are equal. With these two assumptions the total energy transmitted by 5300 A filter is removed from that transmitted by 5577 A filter as a correction for eliminating the background radiation.

The single colour method is based upon the empirical fact that the values of I_z' / I_0' as observed at the base of the atmosphere are largely independent of height for values of z from 0° to about 40° to 50° and for heights 50 and 300 km (the probable range for airglow). The effect of extinction and scattering is not important for small zenith angles. The method assumes that the observed light includes only two components, one from a very high level and the other from some finite height between 50 and 300 km. The contribution from the infinitely high layer to the airglow intensity is uniform all over the sky and not affected by the curvature of the atmosphere. The contribution of this layer is assumed to be F_∞ - a fraction of the zenith intensity, the remaining portion F_u being assumed to originate at a finite height h.

(b) <u>Reduction of observations</u>

The observations were reduced according to following steps for the two colour method.

(1) The intensities in arbitrary units were converted to Rayleighs.

(2) The energy transmitted by 5300 A filter expressed in Rayleighs was appropriately taken out from that

transmitted by 5577 A filter as a correction for the contamination due to the background radiation.

[$E_2 - E_1 = n_2 h\nu_2 - n_1 h\nu_1 = \frac{hc}{2}\left(n_2 - n_1 \frac{\lambda_2}{\lambda_1}\right)$.

For unit deflection n_1 and n_2 are proportional to the calibration factors. The relation indicates that instead of direct n_1, $n_1 \frac{\lambda_2}{\lambda_1}$ should be used for 5300 A filter, i.e. 0.67 instead of 0.014 .]

(2) The residual Rayleighs are slant intensities of 5577 A in different directions of the sky from within the atmosphere without taking into account the curvature of the earth and the extinction coefficient.

Fig.2 represents these slant intensities at different zenith distances to show the variation of OI 5577 A with time on two nights 8-9 January 1959 and 8-9 March 1959. As a broad feature, at a given instant the slant intensities increase with increasing zenith distance. Also in each set the curves are found to be similar in character.

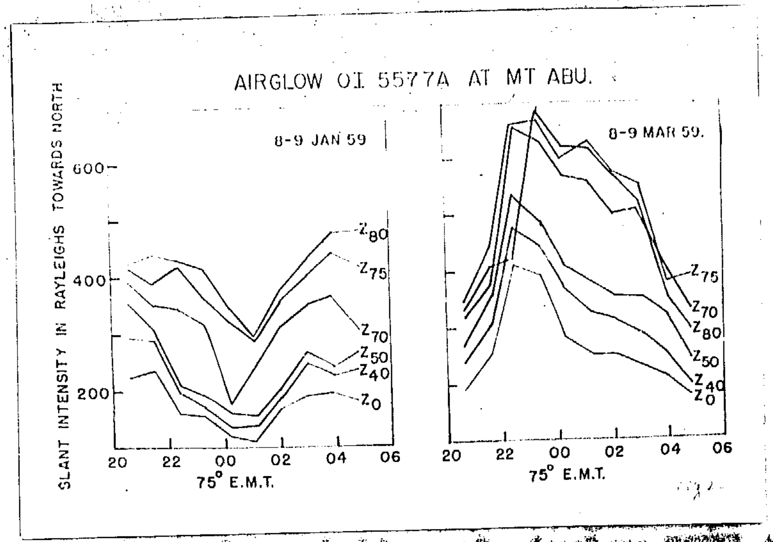

Fig.2. Nocturnal variation of airglow 5577 Å at different zenith angles.

(4) The ratios $I'_z/I'_0 = V'_z$ were determined for each night for zenith distances 40°, 50°, 70°, 75° and 80° from these slant intensities.

I'_z - the intensity at zenith angle z,

I'_0 - intensity at zenith,

V'_z - refers to inside the atmosphere and does not take into account the effect of extinction and scattering.

Table IIa summarises the V'_z values of each night for different zenith distances.

In single colour method, the ratio V'_z is obtained from the direct observations without applying any correction. The value of F_∞ was assumed for each night. The ratios V'_z and F_∞ for the single colour method are presented in table IIb.

Table IIa.

V_z^* for 5577 Å (two colour method).

(V_z^* refers to inside the atmosphere and corrected for the background.)

	Date		V_z^* 40°	60°	70°	75°	80°
1	9-10	Nov.49	1.234	1.451	2.124	2.163	2.034
2	10-11		1.247	1.403	2.040	2.225	2.003
3	11-12		1.253	1.419	2.170	2.340	2.139
4	8-9	Jan.50	1.223	1.378	1.911	2.070	2.008
5	9-10		1.237	1.384	1.901	2.033	2.024
6	11-12		1.263	1.403	1.959	1.991	1.980
7	6-7	Feb.50	1.244	1.401	1.983	2.062	1.960
8	7-8		1.232	1.424	1.982	1.940	1.970
9	8-9		1.224	1.435	2.155	2.204	2.377
10	7-8	Mar.50	1.239	1.399	1.903	2.030	1.905
11	8-9		1.234	1.420	1.983	1.955	1.929
12	9-10		1.243	1.441	2.023	2.193	2.070
13	5-6	Apr.50	1.224	1.439	1.998	2.074	1.994
14	7-8		1.241	1.434	1.934	2.034	1.930
15	8-9		1.239	1.437	1.977	2.004	1.992
∴	Average		1.230	1.423	2.001	2.103	2.000

Height 140 ± 20 km.

Table IIb.

V'_z for OI green line by single colour method.

	Date		V'_z for Z_{70}	Z_{75}	Z_{80}	V_∞
1	9-10	Nov.58	1.732	1.910	1.716	0.23
2	10-11		1.739	1.923	1.814	0.22
3	11-12		1.939	2.074	1.894	0.20
4	8-9	Jan.59	1.633	1.730	1.609	0.35
5	9-10		1.577	1.634	1.593	0.45
6	11-12		1.632	1.678	1.531	0.33
7	6-7	Feb.59	1.690	1.774	1.662	0.34
8	7-8		1.703	1.825	1.768	0.25
9	8-9		1.842	1.833	1.850	0.20
10	7-8	Mar.59	1.777	1.882	1.700	0.25
11	8-9		1.776	1.833	1.730	0.25
12	9-10		1.777	1.930	1.858	0.22
13	3-4	Apr.59	1.879	1.955	1.797	0.20
14	7-8		1.838	1.914	1.807	0.22
15	8-9		1.855	1.932	1.847	0.20

Height 100 ± 30 km.

The dependence of the variation of airglow on the zenith distance is exhibited in Fig.3 by plotting V_g' (from table IIb) against zenith distance.

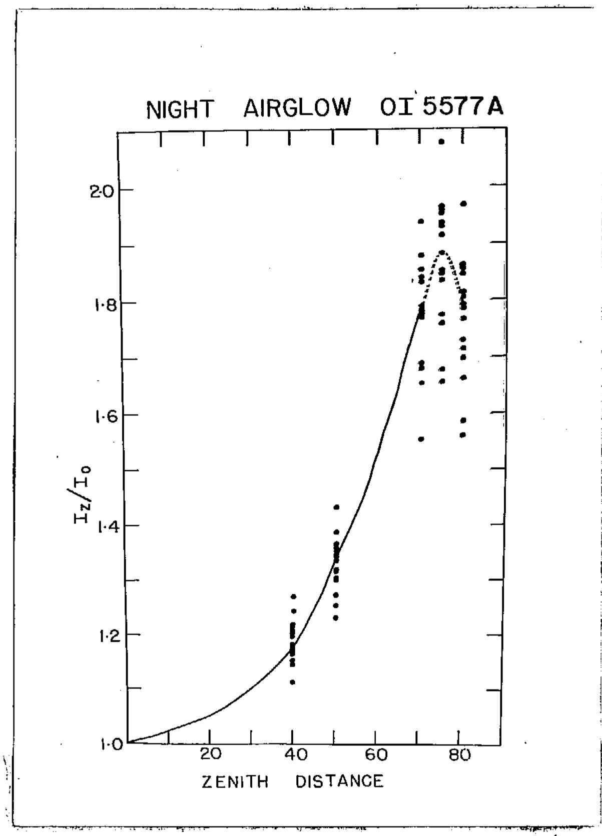

Fig.3. Dependence of V_g' on zenith distance for the OI green line.

The full circles denote the individual values and the curve represents the median. It can be observed that the ratio increases with increasing zenith distance, passes through a maximum and fall towards horizon. The position of the peak depends upon the height of the emitting layer.

The linear diameter of the field of view of the photometer changes with zenith distance. An appropriate correction was applied to the ratios V'_z for eliminating the effect of the finite field of view of the photometer. These are presented in table III. As can be seen the corrections become appreciable for low zenith angles.

Table III.

Correction for the finite field of view of the photometer.

(correction term to be added)

Observed ratios V'_z	Corrections to be applied to V'_{70}	V'_{75}	V'_{80}
1.2	−0.001	+0.002	+0.003
1.3	−0.001	+0.002	+0.004
1.4	−0.001	+0.002	+0.005
1.6	−0.001	+0.003	+0.006
1.8	−0.001	+0.003	+0.007
2.0	−0.001	+0.003	+0.009
2.2	−0.001	+0.004	+0.012

(Taken from Astrophysical Journal 1955, V.122. Corrections were originally determined for a diameter of field 5°. They have been used for the 7° diameter of field.)

(c) The correction for extinction and scattering

If I'_z is the intensity observed at the surface of the earth and I_z the intensity of the same radiation outside the atmosphere, the intensity observed at the surface would suffer an attenuation $e^{-\tau m r_z}$ while passing through the earth's atmosphere, thus -

$I'_z = I_z e^{-\tau m r_z}$ where

τ = extinction coefficient.

m = the air-mass at the observer's zenith (0.83 at Mt. Abu) and

r_z = the relative air-mass at the zenith distance z.

It is necessary to have measurements of the extinction coefficient, for the accurate determination of the height of the emitting layer - unfortunately it is an uncertain factor. Also the magnitude of extinction coefficient appreciably increases due to the presence of haze or dust which may not be easily recognisable by the eye at night. In the present calculations an extinction coefficient $\tau = 0.100$ was used. This value was estimated by Roach et al[6] as the probable upper limit for τ.

For applying the correction due to scattering a value of $\tau = 0.09$ was used corresponding to pure Rayleigh or molecular scattering. This scattering is given by $1 - e^{-\tau m r_z}$.

The effect of the ground albedo is to introduce a small correction to the Rayleigh scattering term. The correction is determined for τ = 0.090 and ground albedo λ = 0.25. The values are taken from Ashburn's[4] tables.

The corrections due to scattering and albedo are summarised in table IV.

Table IV

The scattering functions S'_z

	Corrections S' for the zenith distance			
	z_0	z_{70}	z_{75}	z_{80}
Correction due to Rayleigh scattering				
$(1 - e^{-\tau \sec z})$	0.0743	0.201	0.256	0.352
+ albedo correction for λ = 0.25	0.017	0.045	0.060	0.080
∴ S'_z	0.092	0.246	0.316	0.432

d. The estimation of the height of the emitting layer

Before applying the Van Rhijn formula for determining the height of the emitting layer, the ratios V'_z referred to inside the atmosphere should be converted to V_z referred to outside the atmosphere by taking into account the corrections due to extinction and scattering.

In case of two colour method the procedure leads to the following relation :-

$$V_z = \frac{(V'_z - S'_z)\, e^{\tau m r_z}}{(V'_0 - S'_0)\, e^{\tau m r_z}} \qquad (\tau = 0.180)$$

$$\text{or} \quad V_z = \frac{(V'_z - S'_z)}{(1 - S'_0)}\, e^{\tau m (r_z - r_0)} \qquad .. \quad .. \quad .. \quad (3)$$

where S'_z is the correction due to scattering corresponding to zenith distance z.

The values of V'_z in table IIa were converted to V_z by using relation (3) for determining the height of the emitting layer.

The two colour method yielded a height of 140 $\pm$ 40 km for the layer at which the green line emanates.

In single colour method the two layer hypothesis introduces a term x or P_∞. This modifies relation (3) to

$$V_z = \frac{(V'_z - S'_z)\, e^{\tau m (r_z - r_0)}}{(1 - S'_0)\,(1 - x)} - \frac{x}{1 - x} \quad .. \ (4)$$

Appropriate value of x(or F_∞) was assumed for each night for the determination of V_g from V_g'.

The single colour method furnished a height of 100 ± 30 km for the emission layer of the green line.

(c) Conclusion

It is interesting to compare the results of other investigators. The earlier investigations yielded very high values of the order of 400 to 1000 km for the principal emission lines. This was due to incorrect estimation of the contamination and the extinction due to the earth's atmosphere. For overcoming the effects of contamination Roach[4], and Roach and Meinel[5] suggested two colour and single colour methods. These yielded a height of about 100 km for the green emission layer. Later Roach et al[6], Huruhata and Tohmatsu[7] introduced birefringent filters to eliminate the background radiation. Roach[8] suggested a method of estimating the concordance between the intensity variations at two neighbouring stations. All these workers and Elsasser and Siedentopf[9], Barbier[10] determined a height of 100 km for the emission layer. Rocket observations[11,12,13,14] yielded heights of the same order. The height of 100 km is further supported by theoretical considerations of the excitation mechanism of 5577 Å and also from temperature determinations by the Doppler width of the emission line.

The results obtained at Abu are in reasonable agreement with those obtained by other investigators.

(B) Spatial and temporal variations over the sky

4. General considerations

An attempt was made to study the variation of the distribution of intensity all over the sky. For this purpose the slant intensities obtained by two colour method were converted to local zenith intensities. For this, values V_2' for the zenith distances 40°, 50°, 70°, 75°, 80° were obtained from all the observations available during the period of operation. These values (presented in table IIa) were used for obtaining local zenith intensities from slant intensities.

The geographical coverage of observations made at different zenith distances depends upon the height of the emitting layer. For a given zenith distance, the line of sight would cut a higher layer at a distance further away from the observer's zenith, with the result that the geographical coverage would increase. Table V gives the distance in km away from the observer for various assumed heights and corresponding to different zenith distances. Thus the observation at zenith distance 50° would refer to the zenith of an observer situated at a distance of 117 km along the surface of the earth, if the layer is situated at a height of 100 km, but 228 km away, provided the height of the layer is 200 km. From the table it can be seen that with the height of the layer as 100 km the observations at Abu (upto 60° zenith distance) cover a circular field with a diameter 332 km.

Table V.

Dependence of geographical coverage with the height of the emitting layer.

Zenith distance	Distance along earth's surface to intersection with upper atmospheric layer.		
	h = 100 km	h = 200 km	h = 300 km
0	0	0	0
40	83	161	238
50	117	228	331
70	263	491	693
75	339	616	959
80	436	903	1097

The local zenith intensities were used to study the variations of airglow (a) in the meridian belt and (b) in different directions of the sky.

5. Variations of airglow in the meridian plane

The local zenith intensities in the N-S belt were plotted against time and isophote maps were drawn for each night. Two such isophote maps on 8-9 Jan.59 and 8-9 Mar.59 are presented in Figs.4(a) and 4(b) respectively.

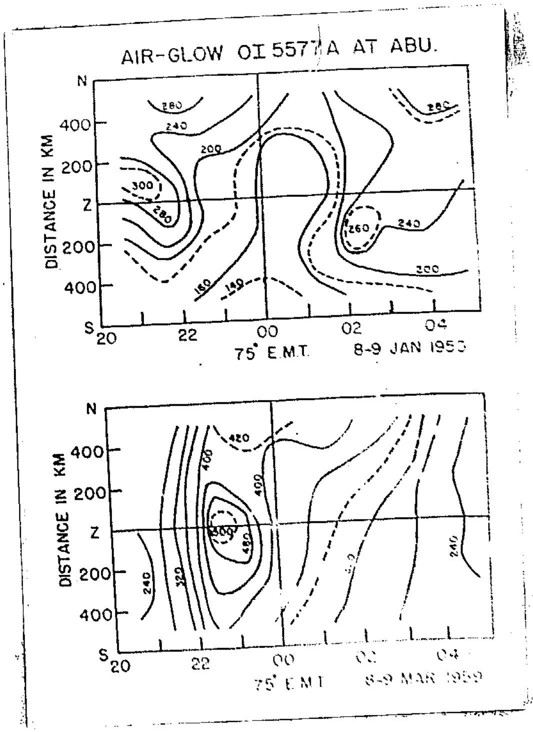

Fig.4. Variation of OI green line over the meridian plane on (a) 8-9 Jan.1959 and (b) 8-9 Mar.1959.

In Fig.4(a) the intensity at the zenith has shown a decrease upto midnight, which is later followed by an increase in intensity towards dawn. The variations in intensity in the N-S belt with respect to time have followed a similar pattern. But it is interesting to study the variations in the N-S belt itself at a given instant. At 2030 hrs the maximum of intensity is slightly away from zenith towards the north and the intensity tapers off on both the sides of the zenith. At 2200 hrs the maximum at zenith is absent and the intensity shows an increasing gradient from south to north. It can be seen from the diagram that the sense of the gradient has remained the same afterwards, but the magnitude has changed from time to time.

Fig.4(b) refers to the night of 8-9 March 1959. Most of the isophote lines are parallel to the north-south direction indicating a uniform intensity all over the belt at a given instant. The intensity all over the belt goes through a maximum at 2300 hrs. At 2000 hrs the intensity is uniform all over the belt, but within half an hour the intensity is maximum at zenith and decreases on either side of horizon. It can also be seen from the figure that there is a tendency for the north to be brighter than south upto 2300 hrs.

Before drawing any conclusions from these meridional maps we shall examine the isophote maps of the whole sky.

6. Nocturnal variation in intensity of the OI green line all over the sky

The local zenith intensities are plotted on projection maps and isophote lines are drawn for each set of observation. Two such series of maps on 8-9 Jan.1959 and 8-9 Mar.1959 are presented in Figs.5(a) and 5(b) respectively.

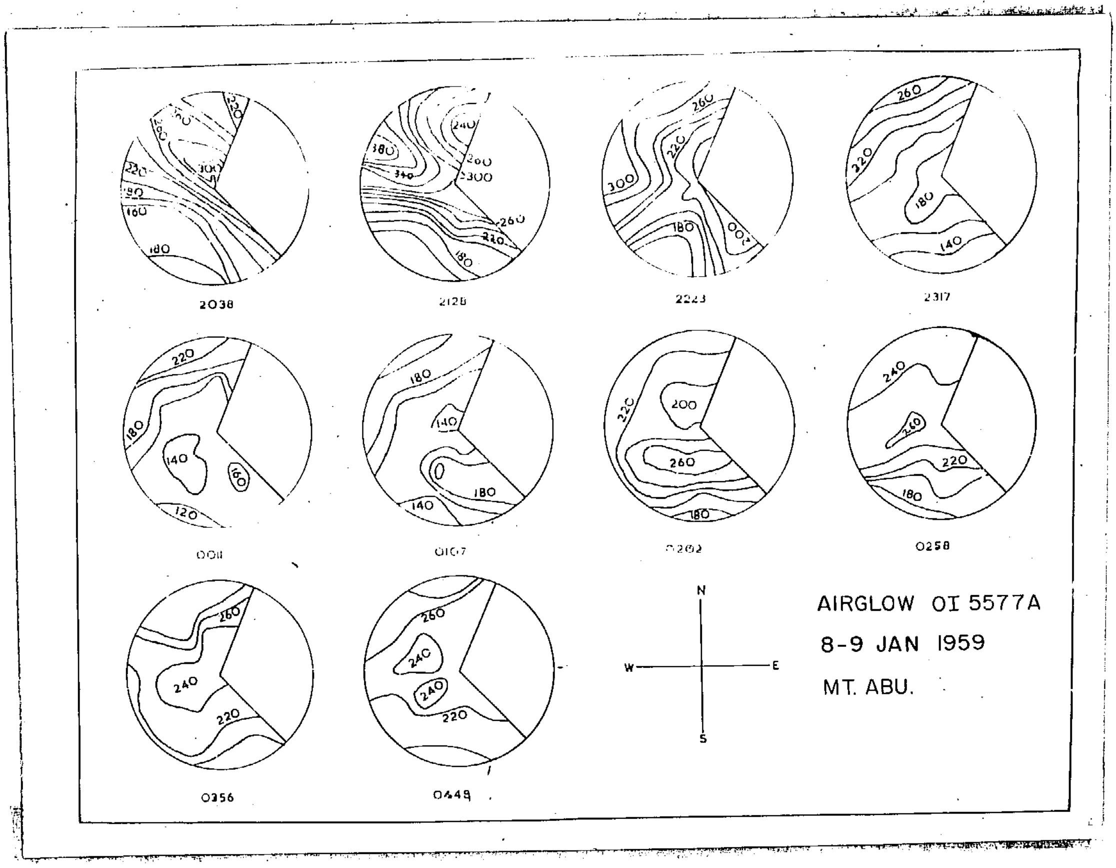

Fig.5(a). Isophote map showing the variation of OI green line over the sky on 8-9 Jan.1959.

As can be seen from table III the maps cover a field of diameter 730 km. A quadrant of each isophote map remains blank, as the observations of that portion are obscured by the building. The directions for the isophote maps are shown at the end of the series. The time of observation is mentioned at the bottom of each map and refers to 75° E.M.T.

In Fig.3(a) the 1st map of 8-9 Jan.1959 shows a maximum of intensity slightly towards the north of the observer's zenith, with the isophote lines running along the N-W S-E direction. In the next hour the distribution on the N-W side has changed producing a maximum in that direction, the distribution over the remaining portion of the sky remaining undisturbed. It may be noticed that the intensity at the N-W horizon is much larger than that at the southern horizon. The next three maps indicate a westward movement of the isophote lines. At 0107 only the southern side has brightened up. The tendency for the maximum is towards the south of the observer's zenith at 0202 hrs. The successive map shows the northward movement with maximum now shifted to zenith. The last two maps represent the existence of practically undisturbed pattern over the sky for two hours before dawn.

The whole series presents a dynamic picture, with an increase in intensity all over the sky for two hours in the beginning of the night. The intensity has reached a minimum at 01 hour and is followed by a slow increase towards dawn.

It may be observed from Fig.3(b) that on 8-9 Mar. 1959 the intensity was practically uniform all over the sky at 2037 hrs. Within an hour a sudden gradient of intensity was developed with a maximum along the S-E N-W belt.

At 2225 hours the intensity increased all over the sky with a maximum at zenith and was followed by a slight over-all reduction in the successive hour. For the next two hours the intensity in the northern region remained unchanged whereas that at the south showed a successive decrease. The steady fall in intensity all over the sky in the later hours could be visualised from the remaining maps.

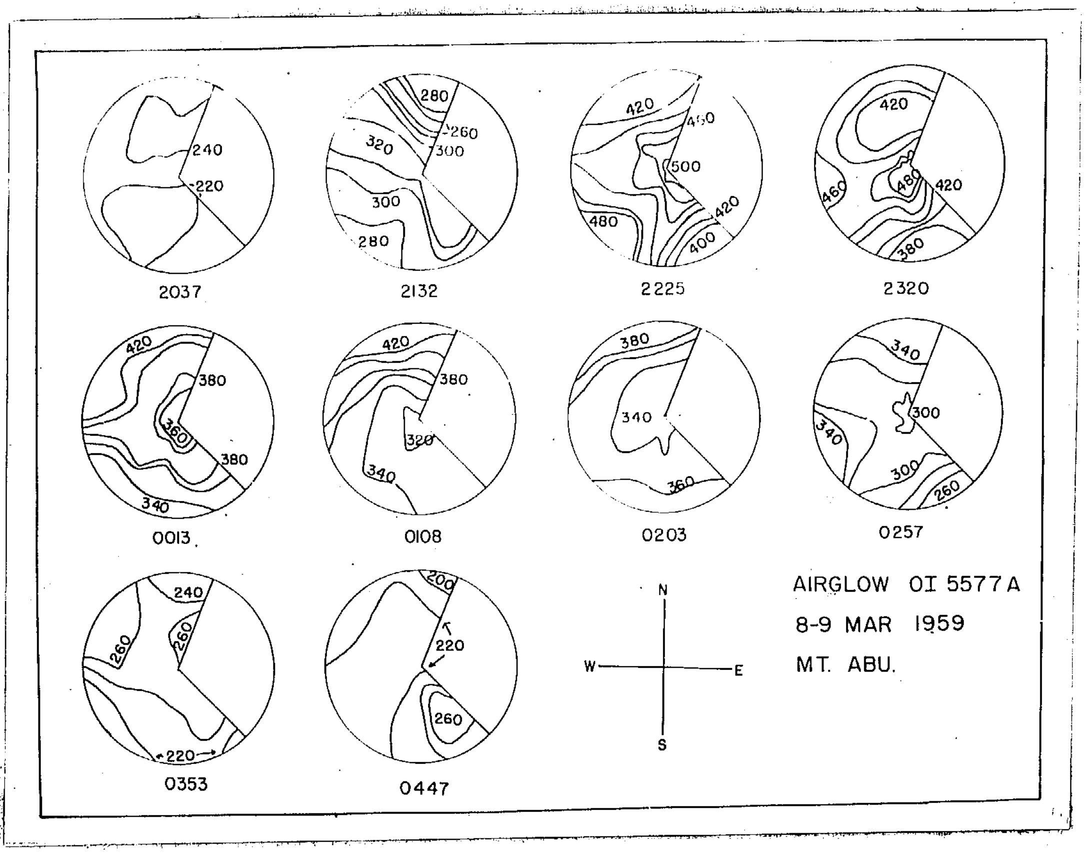

Fig.5(b). Isophoto map showing the variation of OI green line over the sky on 8-9 Mar.1959.

The study of the isophoto maps in the meridional plane and in the whole sky, shows that there is a patchy dynamic structure in airglow. One isophoto map does not show exact similarity with either the previous or the succeeding one. Neither do they show a succession of a single event as suggested by Roach (1961) in his theory of ossified pattern in space, under which observer sees movements. The maps are too few to draw definite conclusions.

7. Estimation of the size of airglow cells

If the existence of the airglow cells is accepted one can obtain a rough estimate of their sizes. Roach et al[15] suggested several methods for this estimation. Out of these (a) rank correlation method and (b) the gradient method were used for estimating the size of the airglow cells, from the data collected at Mt.Abu.

The degree of concordance amongst the simultaneous variations at different points over the sky, was measured by determining the rank correlations. These were found for a series of points in (a) N-S and E-W, and (b) N-E-S and S-E-W planes. The mean values of the rank correlation coefficients 'p' were plotted against the separation between the points and presented in Fig.6. The separation corresponding to p = 0.11 on the graph yielded a value 1110 km, representing the radius of the cell.

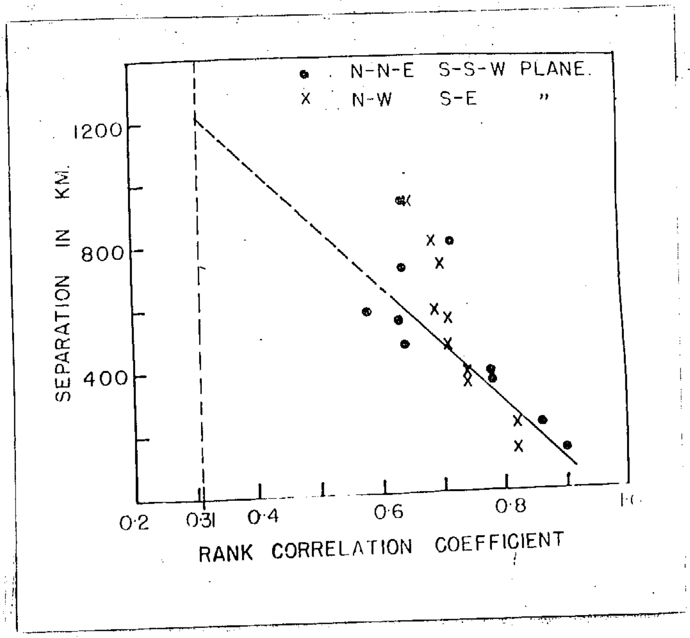

Fig.6. The plot of rank correlation coefficient against separation, for estimating the size of the airglow cell.

The gradient method is based upon the fact that, at a given instant the distribution of intensity over the sky is not uniform, which can be seen from Fig.7. In such case the radius of the cell can be estimated by knowing the maximum and minimum intensities and their separation.

The size of the cell was estimated from each isophote map. From these, an average value of R = radius of the cell was determined for each night. These are summarised in table VI. From table VI it may be concluded that the airglow cell has a radius of about 1125 km.

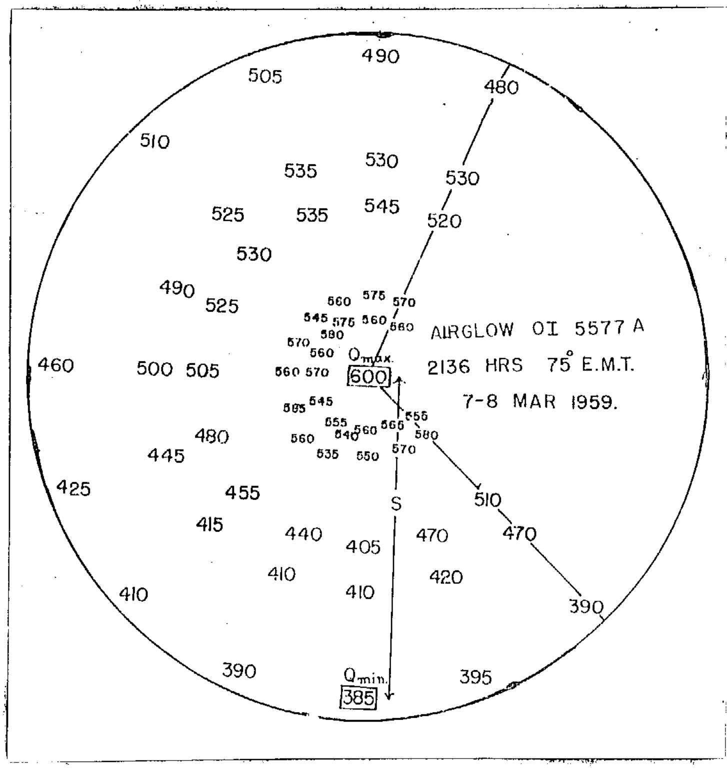

Fig.7. Distribution of intensity of OI green line over the sky.

The results of both the methods can be summarised in brief by saying that the airglow cells have size with diameter of about 2300 km. This is in agreement with the results obtained by Roach et al[15] (1953).

Table VI.

Size of the airglow cells by gradient method.

	Date	Cell size km. (Radius)
1	9-10 Nov.58	965
2	10-11	985
3	11-12	1510
4	8-9 Jan.59	1160
5	9-10	870
6	11-12	995
7	6-7 Feb.59	940
8	7-8	1290
9	8-9	575
10	7-8 Mar.59	1550
11	8-9	1065
12	9-10	1085
13	5-6 Apr.59	1815
14	6-7	960
15	7-8	1310
	Average	1125

REFERENCES

1.	Elvey C.T. and Farnsworth A.H.	1942	Astrophys.J., 96, 451.
2.	Barbier D.	1955	Airglow and the aurorae, Pergamon Press, p.9.
3.	Roach F.E. and Meinel A.B.	1955	Astrophys.J., 122, 530.
4.	Ashburn E.V.	1954	J.Atmos.Terr.Phys., 5, 83.
5.	Roach F.E. and Pettit H.B.	1951	J.Geophys.Res., 56, 325.
6.	Roach F.E., Megill L.R., Rees M.H. and Marovich E.	1958	J.Atmos.Terr.Phys., 12, 172.
7.	Huruhata M. and Tohmatsu T.	1957	Rep.on Iono.Res., Japan, 11, 11.
8.	Roach F.E.	1955	Annales de Geophys., 11, 214.
9.	Elsaesser H. and Siedentopf H.	1956	The airglow and the aurorae, Pergamon Press, p.27.
10.	Barbier D.	1957	Annales de Geophys., 13, 317.
11.	Berg O.E., Koomen M.J., Meredith L. and Scolnik R.	1956	J.of Geophys.Res., 61, 302.
12.	Ibid.	1956	J.of Geophys.Res., 61, 304.
13.	Tousey R.	1958	Annales de Geophys., 14, 186.
14.	Heppner J.P. and Meredith L.H.	1958	J.of Geophys.Res., 63, 51.
15.	Roach F.E., Tandberg-Hanssen E. and Megill L.R.	1958	J.Atmos.Terr.Phys., 13, 113.

CHAPTER V

DAY TO DAY VARIATIONS AND FACTORS AFFECTING THEM

CONTENTS

CHAPTER V

DAY TO DAY VARIATIONS AND FACTORS AFFECTING THEM (Correlations between airglow and other phenomena of the upper atmosphere.)

1. Introduction

The chapter briefly summarises the attempts made to study the correlations between airglow activity and other geophysical phenomena such as magnetic activity, solar activity etc. For convenience, the discussion is made separately for each emission.

2. Geophysical phenomena and the activity of the OI green line

(a) Removal of seasonal variation

Large seasonal changes in the activity of airglow 5577 A are observed. These should be removed if we want to study relations between airglow and phenomena which do not depend on the season. The seasonal variations can be eliminated by treating the data in the following way :-

A mean of three observations at 23, 00, 01 hours local time was obtained for each night, and their monthly mean values were obtained, and also the annual means. The monthly mean value was divided by the yearly mean so as to yield a ratio representative of that month. The observed three hourly intensities were normalised by dividing each value by the factor appropriate for that month. The process removed seasonal variations and all the values formed a scatter about the average intensity of the year. These computed values were used for further analysis. The monthly means, yearly averages and the ratios are summarised in table I.

(b) Effect of magnetic activity

For the study of the effect of magnetic activity on airglow, the K-index data of Alibag magnetic observatory were used. The three hourly K-indices were added over each night only for the night hours. The days were grouped in three categories according to (1) $\Sigma K < 10$, (2) $10 < \Sigma K < 19$ and (3) $\Sigma K \geqslant 19$. The normalised values were put in appropriate groups according to the K_p sums and the mean intensities were found. These were 335, 370 and 330 respectively. From these figures, it may be concluded that the magnetic activity has hardly any effect on the variations of airglow.

Roach and Rees[1] (1960) have observed an increase in airglow with increasing K-index at the high geomagnetic latitude station (64°.6 N) Alaska. Roach[2] (1960) further

Table I.

Normalisation factors for OI 6377 A for eliminating the seasonal variations.

Month	Monthly Mean (R)	Yearly average (R)	Normalisation factor.
Nov.1955	650		0.650
Dec.	443		0.957
Jan.1956	330		1.283
Feb.	305	423	1.391
Mar.	333		1.271
Apr.	530		0.798
May	390		1.083
Jan-Feb.1957	340		1.253
Feb-Mar.	315		1.394
Mar-Apr.	475	425	0.893
Apr-May	465		0.916
May-Jun.	635		0.707
Oct.1957	420		0.833
Nov.	333		1.054
Dec.	270		1.291
Jan.1958	210		1.661
Feb.	245	350	1.430
Mar.	355		0.984
Apr.	430		0.731
May	450		0.775
Jun.	420		0.834
Oct.1958	410		0.876
Nov.	395		0.906
Dec.	310		1.149
Jan.1959	300	360	1.201
Feb.	255		1.398
Mar.	395		0.910
Apr.	475		0.759
May	325		1.099

noticed similar results at the sub-auroral stations Fritz Peak (Geomag.Lat.49°N) and Rapid City (Geomag.Lat.53°N). But the observations at Cactus Peak (Geog.Lat.36°.1N) (Roach[3] 1954) showed a slight negative correlation with magnetic activity, whereas Manring and Pettit[4] (1958) did not observe any correlation between magnetic activity and airglow at the low geomagnetic latitude station (21°N) Sacramento Peak, similar to that at Abu.

Hence it may be concluded that the magnetic activity has hardly any effect on airglow at low geomagnetic stations, but exhibits a better control with increasing K-index in the subauroral and the auroral regions.

(c) Effect of sunspot activity

For investigating the effect of daily sunspot activity on airglow, the normalized data were put in appropriate groups according to the respective Zurich sunspot number. The data for sunspot activity were obtained from CRPL publications. The mean intensities of the groups were plotted against the sunspot numbers. The graph indicated the absence of any relation between airglow and sunspots on day-to-day basis.

It may be mentioned that Roach[3] (1954) did not observe any relation between airglow and sunspot activity for the observations at Cactus Peak. Rayleigh[5] (1928) noticed a positive correlation between airglow activity and solar cycle from observations over a long period of five years.

(d) Effect of solar flares

An interesting result of the effect of solar flares of class 2 + and 3 on airglow can be seen from Fig.1(a) in which six individual cases are shown. Each set shows the intensity of airglow 5577 A on three successive nights, one preceding the solar flare and two following it. The time of occurrence and the size of the solar flare (obtained from CRPL data) are also mentioned in the figure. The increase in intensity on the night following the solar flare may be noted.

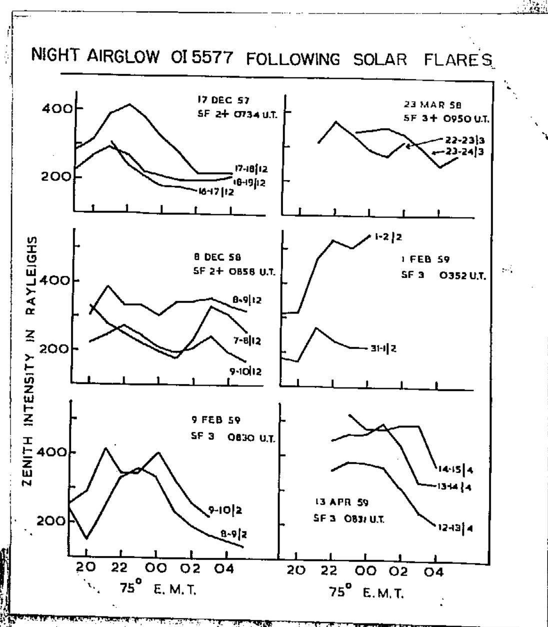

Fig.1(a). Instances illustrating the effect of solar flare on the activity of airglow 5577 A (Mt.Abu).

Similar instances for the observations at Tamanrasset during the I.G.Y. and the I.G.C. period are presented in Fig.1(b).

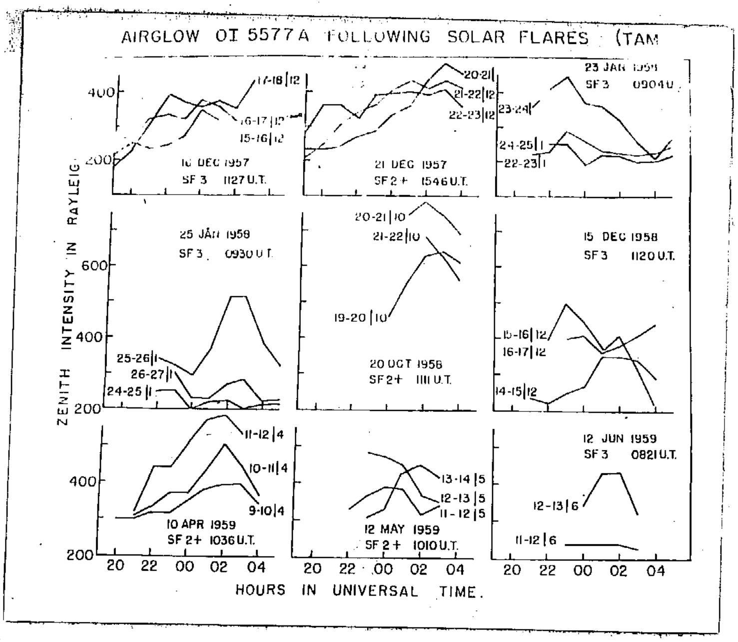

Fig.1(b). Cases exhibiting the effect of solar flares on the activity of OI green line (Tamanrasset).

The observations at both stations, thus lead to the conclusion that the OI green line shows an increase in intensity on the night following a solar flare.

For a further study of the effect of solar flares on the activity of airglow, flares which could be observed at the station between 03 and 10 hours were grouped according to the size of the flares. The results are presented in Fig.2. The full circles represent the mean intensities for the groups and the vertical lines show the error $\sigma/\sqrt{n}$.

The increase in airglow activity is seen to exist with increasing size of the flare.

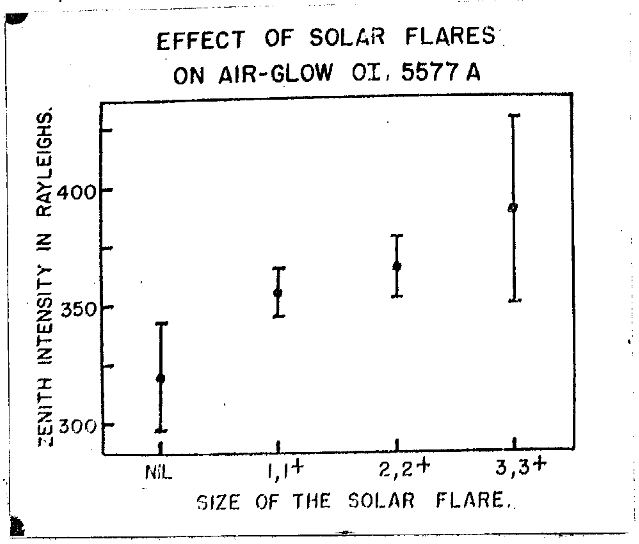

Fig.2. Effect of solar flares on OI green line of airglow (Mt.Abu).

(c) <u>Comparison of day-to-day changes in airglow at different stations</u>

The relation between the day-to-day changes of airglow at two stations would yield valuable information about the spatial extent of correlated variations. Therefore the data at different stations during the I.G.Y., I.G.C. period were compared by the rank correlation method, in the following way:-

(a) Observations at Abu and Tamanrasset.

The mean intensities at three hours 23, 00, 01 local time, at these two stations were compared.

The stations being much separated in longitude the observations are not simultaneous.

(b) Observations at Tamanrasset and Haute Provence. The stations have the same longitude but a large difference in latitude. The simultaneous observations at the midnight hour were compared.

(c) A similar comparison was made between the observations at the Japanese stations. Only a few samples of simultaneous observations were available.

The results are summarised in table II. With reference to table II it is interesting to note that the Japanese stations with separations of about 1000 km yielded a high correlation, whereas the other pairs with separation more than 2000 km, yielded a very low correlation, indicating the absence of any similarity in the day-to-day variations at the latter stations.

Table II.

Comparison of day-to-day variations of OI 5577 A at different stations by rank correlation method.

Stations	Separation in km.	No. of samples	Rank correlation coeff. ρ (Mean)
Abu and Tamanrasset	6700	6	-0.44
Tamanrasset and Haute Provence	2350	12	-0.13
Japanese stations	1000	8	0.81

With the diameter of the airglow cells of about 3300 km, the Japanese stations would have more chances of seeing the same cell as exhibited by the high value of the rank correlation, whereas the stations with separation of the order of the size of the cell or more, would rarely refer to the same cell as shown by the low value of the rank correlation. The results seem to provide an additional evidence for the hypothesis of the airglow cells.

3. Dependence of variations of red airglow on geophysical phenomena

(a) Effect of magnetic and solar activity

For the study of the correlations between red airglow and other phenomena, the data of year 1959 only were used. All the nights with observations at 23, 00, 01 hours local time were considered. From these the mean intensities were obtained. It should be noted that the monthly mean intensities exhibited a variation of 20 % due to seasonal changes.

The data were put into appropriate groups according to :

(a) the K_p sums (for magnetic activity),

(b) the size of the solar flares (for solar activity) and

(c) the daily sunspot numbers (for solar activity).

The mean intensities for the individual groups were determined in each of the above cases. The variation observed for the mean intensities of the groups was about 20 % in each of the cases. This being of the same order as that of the seasonal variations, one can conclude that the activity of the OI red lines is little affected by these factors.

However, in the auroral regions the activity of the OI red lines increases with increasing K-index. It is known to contain substantial auroral component on magnetically disturbed nights (Duncan[6] 1960).

(b) <u>Dependence of airglow red emission on the F layer parameters</u>

An attempt was made to study the relation between the intensity of the OI red lines and (a) f_oF_2 - the critical frequency, (b) h_pF_2 - the height of the maximum electron density and (c) h'F - the minimum height of the F layer.

For this purpose all the hourly night observations of the red airglow at Abu for the year 1959 were used. The ionospheric parameters for the corresponding hours were obtained from the ionograms at a nearby station Ahmedabad (23°.0N, 72°.6E), maintained by the Physical Research Laboratory, Ahmedabad.

Irrespective of the hour of observation the intensities were put into appropriate groups according to the corresponding values of the critical frequencies, each group having an interval of one megacycle. The median values were found for each group. For studying a relation of the form I (6300) = K $(f_oF_2)^n$, the median values were plotted against the critical frequency on a logarithmic scale and presented in Fig.3. The points with $f_oF_2 > 14$ Mc/s are found to lie on one straight line, while those with f_oF_2 below 11 Mc/s lie on a different straight line. The frequencies between 11 to 14 Mc/s form an intermediate case. It is observed that for $f_oF_2 > 14$ Mc/s n is 2 and for $f_oF_2 < 11$ Mc/s n is 0.25.

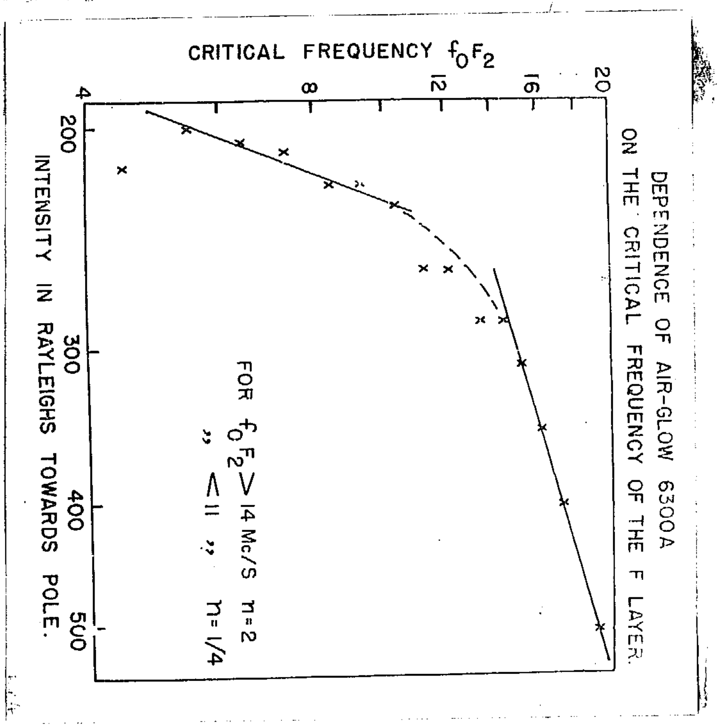

Fig.3. Dependence of red airglow on the critical frequency f_oF_2 of the F layer.

As $(f_oF_2)^n$ represents the maximum electron density of the F layer, the values of n indicate the existence of the control of electron density (n = 2) on airglow for frequencies > 14 Mc/s and practically lack of its control (n = 0.25) for frequencies < 11.0 Mc/s.

For studying the secondary effects such as the dependence of red airglow on the heights h_pF_2 and h'F, the data were treated in two separate groups according to (a) $f_oF_2 > 14$ Mc/s and (b) $f_oF_2 < 11.0$ Mc/s.

To eliminate the principal effect of the dependence of airglow on critical frequency f_oF_2, the quantities $J(6300)/(f_oF_2)^n$ (with appropriate n) were determined from the individual observations. An interval of 20 km was selected for both the heights h_pF_2 and h'F. The values $J(6300)/(f_oF_2)^n$ were put in appropriate groups according to the heights h_pF_2 and h'F. The median value was obtained for each group. These were plotted on a logarithmic scale for deducing a relation of the form $J(6300)/(f_oF_2)^n = K_1 e^{-a_1 h_pF_2}$ and

$J(6300)/(f_oF_2)^n = K_2 e^{-a_2 (h'F)}$, where a_1 and a_2 are constants. The graphs for the median values against h_pF_2 and h'F for the groups $f_oF_2 > 14$ Mc/s and $f_oF_2 < 11$ Mc/s are presented in Figs.4(a), (b), (c) and (d) respectively. Their results are summarised in table III.

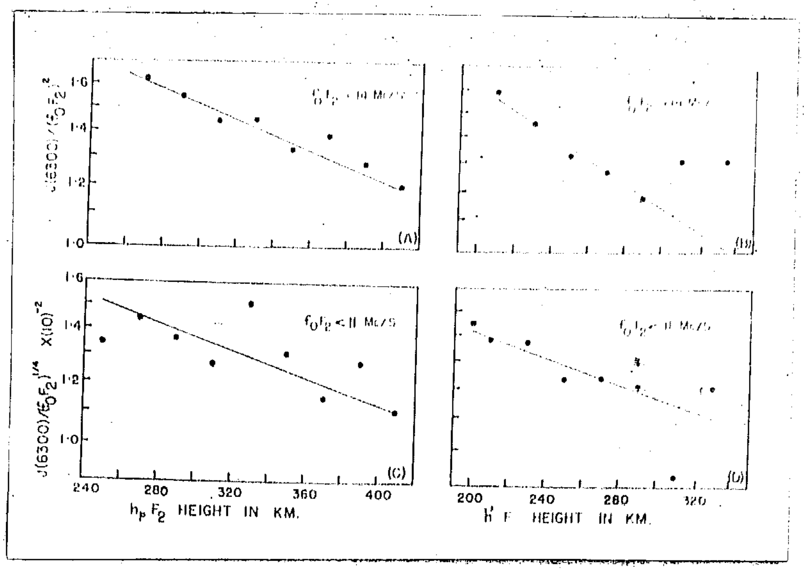

Fig.4. Dependence of red airglow on the heights h_pF_2 and h'F of the F layer.

Table III.

The height dependence of red airglow.

Author	Station	Period	Constants a_1 for h_pF_2	a_2 for h'F	Remarks
Dandekar B.S.	Abu	1959	-0.002	-0.002	for $f_oF_2 < 11$ Mc/s
			-0.002	-0.004	for $f_oF_2 > 14$ Mc/s
Barbier D.[7]	Haute Provence	1956		-0.011	the relation holds only for the 1st part of the night.
Huruhata[8] group	Maruyama	1957-58	-0.004	-0.009	

From table III following conclusions can be drawn:-

(4) The intensity of the OI red lines is proportional to the maximum electron density of the F layer for $f_oF_2 > 14$ Mc/s only. For $f_oF_2 < 11$ Mc/s there hardly exists any relation between the maximum electron density and the red airglow.

(5) The negative values of the constants c_1 and c_2 indicate a decrease in the airglow activity with an increase in the height of h_pF_2 or h'F. The low values show a smaller magnitude for the effect.

For the sake of comparison the results of other investigators are also included in the table.

Barbier[9] (1961) derived an empirical relation

$J(6300) = 6.33\ (f_oF_2)^2 \exp -(h'F - 275)/30$ relating the nocturnal intensity of the OI red lines with the critical frequency of the F layer and its equivalent height h'. But the relation was found to hold only for the 1st part of the night. Huruhata, et al[8] (1959) observed that the OI red radiation is approximately proportional to the maximum electron density of the F layer. Both observed high values for the height coefficients as compared to those found for the observations at Abu. The larger magnitudes indicate a better dependence of the activity of the red airglow on the heights h_pF_2 and h'F at the stations Haute Provence and Maruyama.

REFERENCES

1.	Roach F.E. and Rees M.H.	1960	J.Geophys.Res., <u>65</u>, 1489.
2.	Roach F.E.	1960	J.Geophys.Res., <u>65</u>, 1495.
3.	Roach F.E.	1954	N.B.S.Report, p.3306.
4.	Manring E.R. and Pettit H.B.	1959	
5.	Rayleigh L.	1928	Proc.Roy.Soc., <u>119</u>, 11.
6.	Duncan R.A.	1960	Austra.J.Phys., <u>13</u>, 633.
7.	Barbier D.	1957	C.R.Acad.Sci., <u>244</u>, 2077.
8.	Huruhata M., Nakamura T., Tanabe H. and Tohmatsu T.	1959	Rep.Iono.and Space Res., Japan, <u>13</u>, 283.
9.	Barbier D.	1961	Ann de Geophys., <u>17</u>, 3.

CHAPTER II

GENERAL DISCUSSION AND NEED FOR FURTHER WORK IN TROPICS.

CHAPTER VI

GENERAL DISCUSSION AND NEED FOR FURTHER WORK IN TROPICS

In the preceding chapters, we have described the equipment used, its calibration, the method of reducing the data and the results which have come out. The data at Abu have been compared with those at a few other stations.

The nocturnal variations of all the three radiations under study have been found to differ from one another. The OI green line exhibits a midnight maximum, with the hour of occurrence changes with season. The OI red lines show a post-twilight decrease in intensity. The intensity of Na-D lines is observed to remain more or less constant during night with a slight decrease towards dawn.

The seasonal variations of OI green line possess two maxima one in autumn and the other in spring and a minimum in winter.

Unfortunately nothing definite is known about the variation during the monsoon period June to September. But there are indications of another minimum in that season.

The study of isophote maps reveals the patchy nature of airglow and the existence of movements. A tentative estimate of the size of airglow cells has yielded a diameter of about 2500 km which is of the same order as that found by other workers.

Magnetic and sunspot activities do not produce any significant effect on the variations of intensity of the OI green and red lines. There is however evidence of the enhancement of airglow intensity due to solar flares in the case of OI green line. The intensity of the OI red lines is found to depend on the critical frequency f_oF_2 and the heights h_pF_2 and h'F of the F layer.

Although some of these broad features of tropical airglow have been ascertained, there is great scope for further work, and also for the improvement in the work done at Abu.

As can be seen the instrument used in these investigations used rather broad band optical filters. This has introduced errors in the observations owing to background radiation. The effect could be reduced by using narrow band interference filters or birefringent filters such as those by Dunn and Manring[1], Roach et al[2] and others[3]. The possibility of using spectroscopic technique also requires to be explored. Barbier[4] has used an eight colour photometer and studied the correlations amongst the intensities at different wavelengths to eliminate this contamination.

Commercial radioactive sources are known to be temperature dependent. To check the stability of the equipment over long periods, frequent calibrations are necessary. This is important because the electronic equipment and the optical filters used may not retain the same character over a long range of years. Further the effect of the finite field of view of the photometer and of extinction and scattering in the atmosphere should be properly estimated.

For studying effects of solar activity on airglow it is essential to collect data over a long period of years. In the auroral zone the intensity of airglow is known to increase with increasing magnetic activity, whereas there is hardly any effect due to changes in magnetic activity on airglow variations in low latitudes. The study of the dependence of airglow variations with changes in magnetic activity with latitude should prove interesting if more data are collected.

The study of airglow has received insufficient attention especially in low latitudes. A few stations from the geographic or geomagnetic equator to middle latitudes will prove valuable, for problems like the determination of the height of the emitting layer, the nature of airglow movements and their latitude dependence. The selection of these stations should be such as to reduce serious gaps in the data due to the monsoons.

The OH bands have not been studied in the tropics. Na-D and OI red lines need further attention.

REFERENCES

1.	Dunn R.B. and Manring E.R.	1956	J.O.S.A., 46, 572.
2.	Roach F.E., Megill L.R., Rees M.H. and Marovich E.	1958	J.Atmos.Terr.Phys., 12, 171.
3.	Manring E.R. and Pettit H.B.	1956	The airglow and the aurorae, Pergamon Press, p.29.
4.	Barbier D.	1956	The airglow and the aurorae, Pergamon Press, p.38.

PUBLICATIONS

1. An Experimental arrangement for scanning Night Airglow over the sky.

2. Preliminary report on Airglow observations on 5577 A made at Mt. Abu (24^{o}.6N) in 1957-58 (Abstract).

3. Study of Night Airglow at Mt. Abu OI - 5577 (Abstract).

4. Night Airglow at Mount Abu OI - 6300 A (Abstract).

An Experimental arrangement for scanning Night Airglow over the sky

By

B.S.Dandekar

and

R.V.Bhonsle,

Physical Research Laboratory, Ahmedabad-9.

A B S T R A C T

The note describes the construction and working of a scanning unit for measuring the airglow at different altitudes in a vertical plane.

Sample records are presented.

(Accepted by the Indian Journal of Scientific and Industrial Research for publication.)

An Experimental arrangement for scanning Night Airglow over the Sky

By

B.S.Dandekar and R.V.Bhonsle,
Physical Research Laboratory, Ahmedabad.

From January 1956, we have been recording at Mt.Abu the night airglow intensities of OI green line 5577 A and the background emission at 6300 A with an RCA 931-A photo-multiplier, two narrow band interference filters, a D.C. amplifier and a 0-1 mA Evershed pen-recorder. The airglow intensities have been recorded continuously on most of the clear moonless nights. The photometer was directed towards the celestial-north pole. The observations have proved useful for studying the nocturnal and the seasonal intensity variations of 5577 A in the airglow.

To study such problems as the determination of the height of the emitting layer by Van Rhijn's method, or the variation of the airglow in different directions, it is essential to scan the whole sky with a photometer[1] either manually or automatically. It would be best to arrange fully automatic scanning over all azimuths and altitudes such as has been done by Marlow and Pemberton[2] (1949), Baillet, D.Barbier et al[3] (1953), Elsasser and Siedentopf[4] (1956), and others[5,6] using automatic scanning systems. But as it was found difficult to make a fully automatic equipment with the available resources, a simple scanning unit for operating in any given vertical plane was constructed.

It is the purpose of this note to describe the construction and working of this meridian scanning Airglow Photometer built at the Physical Research Laboratory, Ahmedabad and used at Mount Abu.

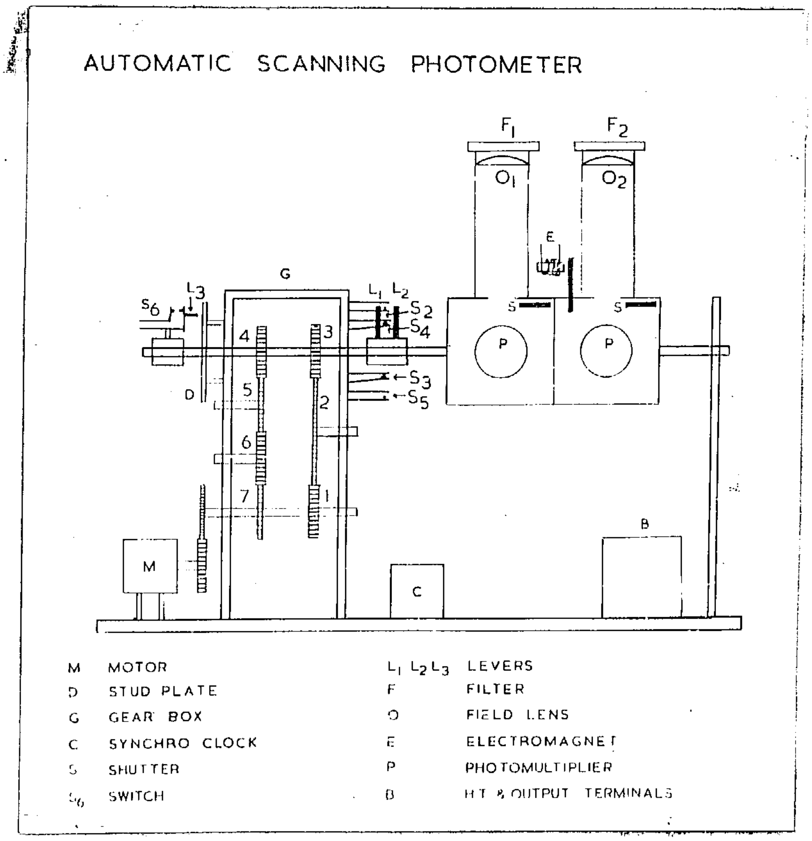

Fig.1. General arrangement of scanning photometer.

Fig.1 shows a schematic diagram of the fixed vertical circle scanning photometer. It consists of a box made of thin aluminium sheet containing two exactly similar RCA 931-A photomultipliers (P_1 and P_2). The lenses (O_1 and O_2) define the field of view of the photometer. Each photometer has a circular field of 6° diameter. Two filters (F_1 and F_2) are mounted in front of the lenses O_1 and O_2. F_1 transmits mainly the OI green line 5577 A and F_2 transmits background radiation in the region 5300 A. Shutters (S & S) can cut off the light from the phototubes and they can be operated from outside by a lever pulled by an electromagnet E. The photometer box is mounted on a horizontal axis and is rotatable in a vertical plane. A synchronous motor M is coupled to the rotatable photometer box through the gears in box G.

The photometer scans the sky in the meridian plane from north to south. In the succeeding scan, the photometer rotates in the reverse direction. The reversal of direction is achieved by the use of appropriate gearing. The scanning can be either continuous or at definite predetermined intervals. For obtaining the scan at definite intervals, a synchronous clock C is used. It runs directly on 230 V 50 C/s and normally gives half hourly contacts. The lever L_1 mounted on the axle of the photometer opens the switch S_2 or S_3 in the end position of the scan and thereby stops the motor M by cutting off its supply. The next scan is initiated by the clock C. The lever L_2 energises the electromagnet E at the beginning and end of the scan by pressing the switch S_4 or S_5 thereby operating the shutter S. A series of studs are mounted on a semicircular plate D at intervals of 20° of the scan. The studs press the lever L_6 successively and momentarily close the switch S_6 during the scan. This provides angular position marks on the chart, and records the levels of dark current of the photomultiplier.

The supply of H.T. voltage to the phototubes is made by flexible wires connected to a small insulated box B. This avoids the twisting of the wires due to the rotation of the photometer.

The output voltages are amplified by a three stage d.c. amplifier and are fed to a 0.1 mA Evershed twin-pen recorder. One scan takes about 3½ minutes.

The constituent parts which perform the scanning operation are (1) the gear box and (2) the switching system. We shall consider these in a little more detail.

The gear box

It consists of two sets of toothed wheels of equal diameter as shown in Fig.2. One set of wheels Nos.1, 2, 3 rotate the photometer in a clockwise direction and the other set comprising wheels 4, 5, 6, 7 rotate the system in the anticlockwise direction. The wheels 1 and 7 are mounted on the shaft of the driving motor and wheels 3 and 4 are on the axle of the photometer. The coupling between the photometer and the driving shaft is provided either by wheel No.2

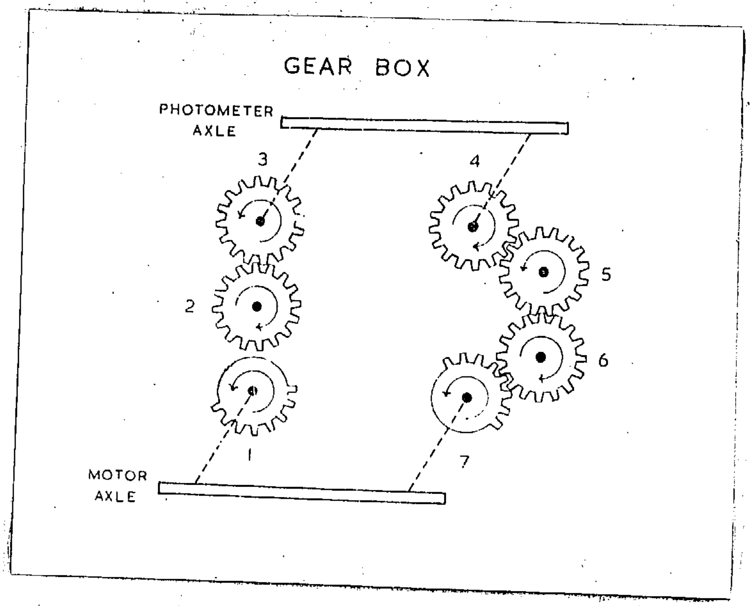

Fig.2. Gear system for reversing the scan.

or wheels 5 and 6. Half the teeth of the wheels 1 and 7 are removed in such a way that they avoid the simultaneous coupling of the axles through both sets of wheels. The shaft of the motor rotates in a clockwise direction at a speed of eight minutes per rotation. The motor shaft drives the photometer axle either through wheels 1, 2, 3 or through 4, 5, 6, 7 depending on whether wheel 2 or 6 is engaged with the motor driven wheel 1 or 7. The reversal of direction of the photometer axle is due to the additional wheel No.5 in the second set. The gear system enables the photometer to scan the sky upto 80° on either side of the zenith.

<u>The switching system</u>

The switching system is divided into two parts, one for the automatic start and stop of the scan, and the other for operating the shutter.

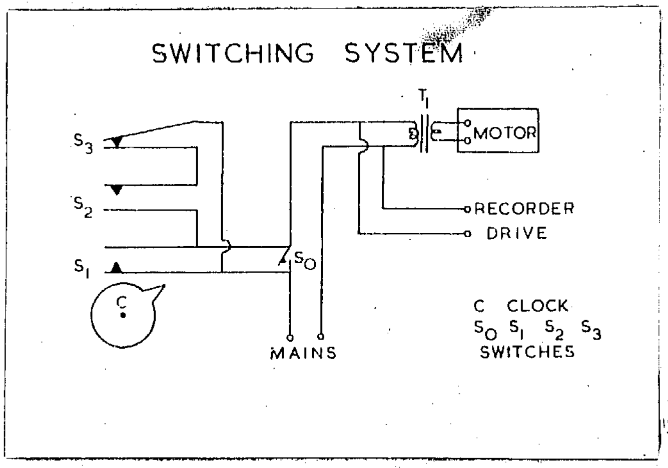

Fig.3(a). Circuit diagram for the automatic starting and stopping of scan.

Fig.3(a) shows a schematic arrangement of the switching system. The switch S_o allows continuous scanning operation. The clock C with switch S_1 puts the unit on at regular intervals, whereas the switching at the end of the scans is achieved through the switches S_2 and S_3 which are operated by the lever L_1 of Fig.1.

The shutter system

The shutter system is presented in Fig.3(b). The switches S_4 and S_5 which are operated by the lever L_2 (of Fig.1) expose the photometer to sky only during the

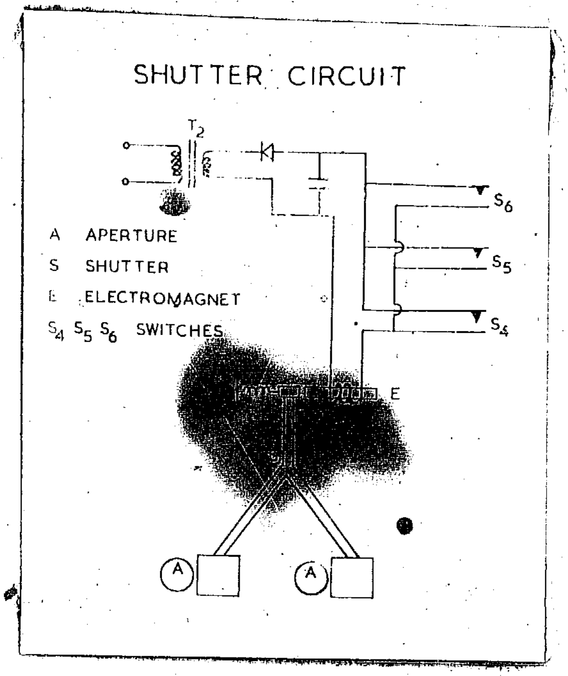

Fig.3(b). Arrangement for operating the shutter.

scanning operation. The switch S_6 is operated by the lever l_3 (Fig.1) at every 20° interval during the scan to provide angle marks on the chart.

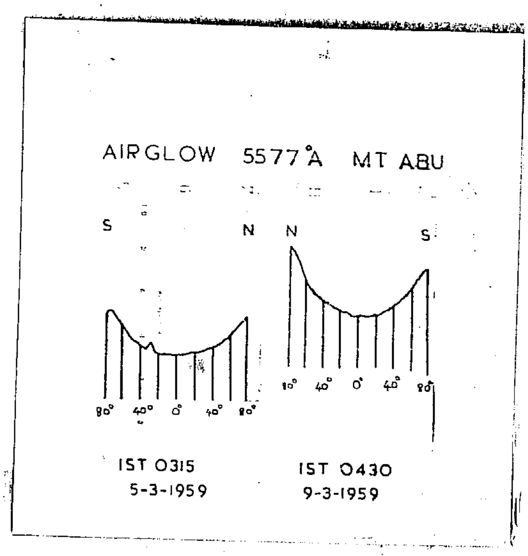

Fig.4(a)&(b). Sample records showing the variations of intensity of airglow 5577 Å in the meridian plane.

Fig.4 shows sample records of the variation of the intensity of airglow 5577 Å observed at Mount Abu with this instrument in the meridian plane. The bump in Fig.4(a) at 30°S is due to the presence of a star in the field of view of the photometer. The records clearly show that the intensity of airglow is minimum at the zenith and increases towards horizon.

Applications of the Instrument

The instrument has been found to be of use for studying the following problems :-

(1) The variations of airglow intensity in a given vertical plane.

(2) The determination of the height of the emitting layer by Van Rhijn technique.

(3) The photometry of the zodiacal light and of the gegenschein.

Acknowledgements

Our thanks are due to Dr.K.R.Ramanathan, Director, Physical Research Laboratory for encouragement and providing us with all the necessary facilities for the work. The authors

(S.S.Dandekar and R.V.Bhonsle) were receiving maintenance grants from the Council of Scientific and Industrial Research and the Department of Atomic Energy of the Government of India respectively.

REFERENCES

1. Roach F.E. 1956 Instruction Manual (IGY) No.IV Aurora and Airglow.
2. Marlow D. and Pemberton J. 1949 Rev.Sci.Instr., 20, 724.
3. Baillet A., Barbier D., Dossen R., Lallemand and Maguery J. 1953 Ann de Geophys., 9, 309.
4. Elsaesser H. and Siedentopf H. 1955 The Airglow and the Aurorae, Pergamon Press, p.57.
5. Roach F.E. and Pettit H.B. 1951 J.Geophys.Res., 56, 325.
6. Huruhata M., Tanabe H. and Nakamura T. 1955 The Airglow and the Aurorae, Pergamon Press, p.80.

Preliminary report on Airglow observations on 5577 Å made at Mt.Abu ($24^{\circ}.6$ N) in 1957-58

By

B.S.Dandekar, R.V.Bhonsle and K.R.Ramanathan,
Physical Research Laboratory, Ahmedabad-9, India.

A B S T R A C T

In this report, the observations on airglow intensities on 5577 Å made at Mt.Abu ($24^{\circ}.6$ N) towards the pole in the first half of 1957 and 1958 are summarised. There are significant diurnal and seasonal variations. In the winter months, the maximum intensity occurs one or two hours before midnight, while in the equinoctial months March-May, the maximum intensity occurs at a later hour, shortly after midnight, and its value is also greater. There are large day-to-day variations of intensity in all the months.

(Presented at the Moscow Conference)

Study of Night Airglow at Mount Abu OI - 5577

By

B.S.Dandekar,

Physical Research Laboratory, Ahmedabad-9, India.

A B S T R A C T

An airglow observation station was started by the Physical Research Laboratory, Ahmedabad, at Mt.Abu (Geog. Lat.24°.6 N, Long.72°.7 E) in December 1955. The paper describes the instrumentation used and discusses diurnal and seasonal variations of the OI green line in the airglow. The variations in intensity are found to have no correlation with either sunspot or magnetic activity. An increase in the intensity of OI 5577 A was observed on the night following a number of solar flares.

(Presented at the I.G.Y. Symposium, February 1961.)

Night Airglow at Mount Abu OI - 6300 Å

By

B.S.Dandekar,

Physical Research Laboratory, Ahmedabad-9, India.

ABSTRACT

The note describes the photometer used for studying the OI red lines of the airglow at Mt.Abu and the calibration of the photometer against a standard tungsten filament lamp.

The nocturnal variations of the red airglow in different seasons are discussed and compared with those occuring at another station Haute Provence.

The intensity of the OI red lines is shown to increase with an increase in the critical frequency of the F layer. The rate of increase is enhanced when the critical frequency exceeds 14 Mc/s.

(Presented at the I.G.Y. Symposium, February, 1961.)